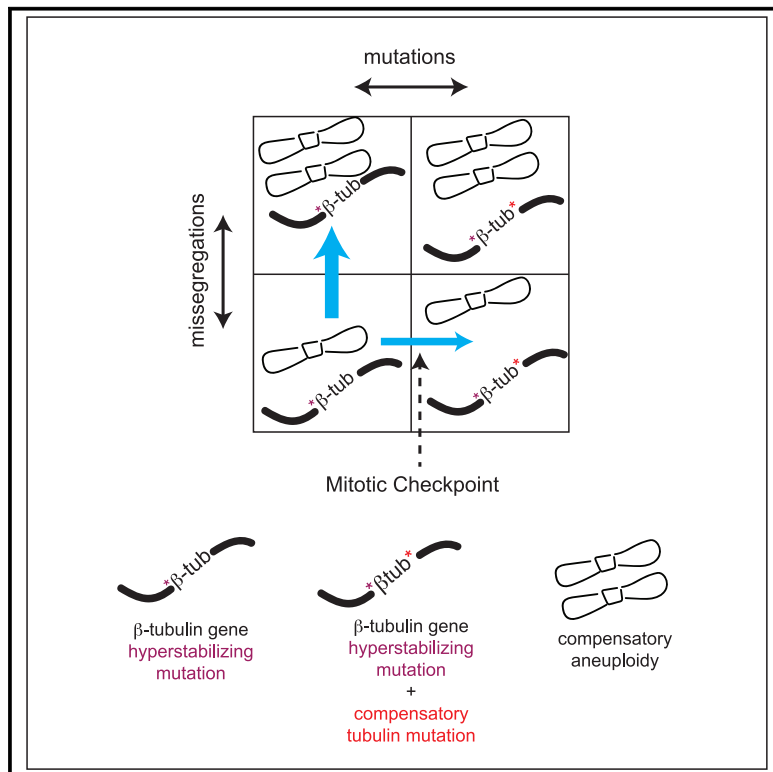


Evolutionary adaptation to hyperstable microtubules selectively targets tubulins and is empowered by the spindle assembly checkpoint

Graphical abstract



Authors

Francesca Macaluso, Tasia Bos,
Elena Chirolì, ..., Simone Pompei,
Luke M. Rice, Andrea Ciliberto

Correspondence

andrea.ciliberto@ifom.eu

In brief

Cells acquire compensatory mechanisms to cope with insults altering microtubule dynamics. Macaluso et al. show that, while most euploid cells become aneuploid, a small fraction of cells acquires compensatory mutations that are fixed in the population. All mutations restoring growth restore microtubule dynamics, although to varying degrees.

Highlights

- Yeast cells hyperstabilizing microtubules acquire aneuploidies and tubulin mutations
- Aneuploidies are evolutionary diversions, as mutations originate from euploid cells
- Compensatory mutations restore microtubule dynamics to varying degrees
- The mitotic checkpoint increases the target size of compensatory mutations



Article

Evolutionary adaptation to hyperstable microtubules selectively targets tubulins and is empowered by the spindle assembly checkpoint

Francesca Macaluso,¹ Tasia Bos,² Elena Chirolí,¹ Paolo Bonaiuti,¹ Jason C. Apuan,² Fridolin Gross,³ Simone Pompei,¹ Luke M. Rice,² and Andrea Ciliberto^{1,4,5,*}

¹IFOM-ETS, The AIRC Institute of Molecular Oncology, Via Adamello 16, 20139 Milan, Italy

²Departments of Biophysics and Biochemistry, UT Southwestern Medical Center, Dallas, TX 75390, USA

³ImmunoConcEpT, CNRS UMR5164, Université de Bordeaux, 33076 Bordeaux, France

⁴Pázmány Péter Catholic University, Faculty of Information Technology and Bionics, 1083 Budapest, Hungary

⁵Lead contact

*Correspondence: andrea.ciliberto@ifom.eu

<https://doi.org/10.1016/j.celrep.2025.115323>

SUMMARY

Microtubules are polymers required for chromosome segregation. Their drug-induced hyperstabilization impairs chromosome segregation and is an established anti-cancer therapy. How cells respond to microtubule hyperstabilization, however, is incompletely understood. To study this, we evolved budding yeast cells expressing a microtubule-hyperstabilizing tubulin mutant and isolated adapted strains. Aneuploidy of specific chromosomes carrying the microtubule regulators *STU2* and *VIK1/KAR3* was the first observable adaptation. In the longer run, aneuploidies were outcompeted by mutations in α - or β -tubulin, partially overlapping with mutations in cancer patients. Thus, compensation of microtubule hyperstabilization follows a restrained and reproducible path where new mutations combine with the original offending mutation on the same carrier. While partly compensatory, several mutations failed to re-establish fully normal microtubule dynamics. Sustained growth relied on the mitotic checkpoint, indicating that extended mitotic timing limits the genomic instability caused by reduced microtubule dynamics. Our results predict a potential vulnerability of cells resistant to microtubule-hyperstabilizing agents.

INTRODUCTION

In nature, organisms often face variable conditions that can cause reduction of the reproductive ability of individuals. This can be mitigated by compensatory mutations that allow recovery of fitness, at least partially. Such mutations are selected during a process known as adaptive or compensatory evolution. The dynamics of this process are studied in laboratories by evolution-repair experiments,^{1,2} which have been used to examine, for example, the evolutionary response to mutation-induced impairment of key cellular processes² and specifically DNA replication,^{3,4} bud formation,⁵ error correction in chromosome segregation,⁶ cytokinesis,⁷ and more. These experiments have shown that cells typically recover normal growth within a few hundred generations. Compensatory changes can occur via point mutations but can also be the result of large genomic re-arrangements such as aneuploidy. While aneuploidy has typically detrimental effects on an individual's reproductive fitness, it can also have an adaptive effect under stressful conditions via an increased dosage of specific genes (see, for example, Rancati et al.⁷ and Yona et al.^{7,8}). Point mutations offer alternative evolutionary routes to aneuploidy but, although offering fitter solutions, they occur at a lower rate. Hence, while aneuploidy offers a quick

response to external stimuli, it can be replaced in the medium term by point mutations.^{7–11} Point mutations are usually hypomorphic and span many functional modules, showing the elevated plasticity of evolutionary processes even when conserved functions are altered.^{1–3,5} In some cases, rather than recovering lost modules, cells “invent” new ways to perform the impaired function.⁷

Impairment of key cellular functions can also be caused by drug treatment, to which cells often respond with the emergence of resistance mechanisms, again mediated by compensatory mutations.¹² Hence, understanding the process of compensatory evolution may shed light on how cells cope with drugs that target key cellular functions. In particular, here, we ask how cells cope with hyperstabilization of microtubules, which are polymers of $\alpha\beta$ -tubulin and a core structural component of eukaryotic cells.¹³ Microtubules are essential for chromosome alignment and provide the mechanical force for chromosome segregation; accordingly, aberrant microtubule dynamics can lead to chromosome mis-segregation.^{14,15} For sister chromatids to be separated, they need to be pulled by microtubules emanating from the two centrosomes at opposite poles of the spindle. Ensuring successful chromosome segregation is the task of regulatory control mechanisms; the chromosome passenger complex



(CPC), which includes the protein kinase Ipl1 (Aurora B in mammals),¹⁶ destabilizes attachments when kinetochores are not under tension, and the mitotic checkpoint arrests cell cycle progression upon lack of tension or attachment.¹⁷ Only when all kinetochores are attached and under tension is the mitotic checkpoint satisfied, which licenses progress into anaphase. In higher eukaryotes, microtubules can be hyperstabilized; for example, by treatment with drugs widely used in cancer treatment, such as taxanes.¹⁸ Upon Taxol treatment, mammalian cells arrest in mitosis in a mitotic checkpoint-dependent manner.¹⁹ As a consequence of the arrest, cells can either die or transit into anaphase while mis-segregating chromosomes, an event that impacts their viability.^{20,21}

How cells react to treatments that hyperstabilize microtubules is incompletely understood. Here, we addressed this question in the budding yeast *S. cerevisiae*. Budding yeast is not sensitive to taxol,²² but yeast microtubules are stabilized in an apparently similar way by a well-characterized point mutation, *tub2*^{T238A}, in *TUB2* (β -tubulin in humans).^{23,24} This mutation is buried within the protein and stabilizes microtubules through an allosteric mechanism. It does not directly alter tubulin:tubulin polymerization contacts or sites of interaction with other tubulin-binding factors. Since the *tub2*^{T238A} mutation does not have a permissive temperature, cells expressing this mutation are strongly impaired in growth.²³ Our results show that, besides temporary aneuploidies, cells adapt to hyperstable microtubules exclusively via mutations in α - and β -tubulin that restore microtubule functionality. Compensatory mutations in other proteins or modules are not observed. This univocal pattern of compensatory mutations suggests that the evolutionary adaptability of the microtubule regulatory apparatus is limited. At the same time, our results identify the mitotic checkpoint to be essential for growth of cells with tubulin mutations that do not entirely restore normal microtubule dynamics. Given the high degree of tubulin conservation in eukaryotes, our results have implications for understanding the emergence of resistance to taxanes in human cancers.²⁵

RESULTS

Yeast cells recover growth when microtubules are hyperstabilized

To examine the evolutionary response to microtubule hyperstabilization, we took advantage of the point mutation *tub2*^{T238A}. In contrast to using drugs to stabilize microtubules, using a buried mutation should not elicit commonly observed responses, such as mutations in multi-drug transporters, and/or suffer from off-target effects.

As expected from prior work,²³ *tub2*^{T238A} haploid cells were strongly impaired for growth at different temperatures (Figure S1A). Since these cells have a strong growth defect and do not show a permissive condition, we could not directly use haploid cells for the evolution experiment. Instead, we noticed that the mutation was recessive because heterozygous *TUB2/tub2*^{T238A} did not show aneuploidies (Figure S1B) and grew similarly to the diploid wild type (Figure S1C). Hence, we sporulated the heterozygous diploid to obtain wild-type (WT) and *tub2*^{T238A} haploid strains, which were the starting point of the evolution experiment. *tub2*^{T238A} cells were viable but formed

smaller colonies than the WT (Figure 1A). If this phenotype was related to chromosome mis-segregation, then we expected an even more severe effect when the mitotic checkpoint was deleted. Indeed, *tub2*^{T238A} *mad2Δ* haploids were dead (i.e., did not even give rise to small colonies) (Figure 1B). This result suggests that *tub2*^{T238A} cells undergo numerous errors in microtubule-kinetochore attachment that, if not corrected by the checkpoint, preclude cell viability.

Once WT and *tub2*^{T238A} colonies reached a sufficient size (2 and 3 days, respectively), they were transferred to liquid culture to continue the evolution experiment. The moment of transfer to liquid medium was denoted as the first time point (hereafter called T0) when we counted the number of generations (Figure 1A). Throughout the experiment, cells were grown in a 96-well plate and diluted daily to optical density (OD) 0.05. Growth rate was assessed every 2–3 days. To capture potential variability in the adaptive response, we evolved 5 WT and 21 *tub2*^{T238A} populations in parallel.

We measured growth rates as a readout of evolutionary adaptation. We also kept track of cell size, DNA content, and microtubule morphology throughout the experiment. Whereas, at the beginning of the experiment, the growth rate of *tub2*^{T238A} was strongly impaired compared to the WT, it started to increase after ~50 generations, approaching that of the WT after ~65 generations. The mutants maintained this growth rate until approximately generation 190, at which point (referred to as Tf) we stopped the experiment (Figure 1C). Also, cell size, DNA content, and microtubule morphology of ancestor *tub2*^{T238A} cells differed from the WT. Measurements were done after 48 h of growth in liquid (defined as T1; Figure 1A). In line with growth rate measurements, these cellular features also approached WT levels at the end of the experiment (Figures S1D–S1F).

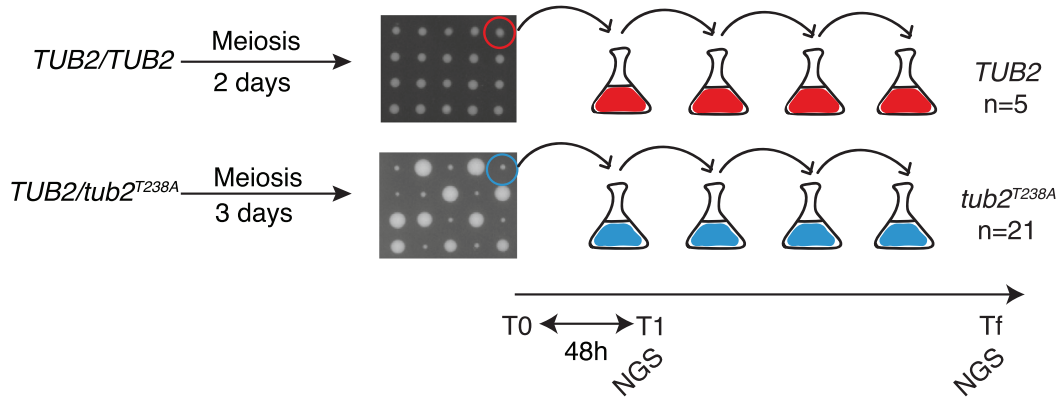
Thus, cells evolved to compensate for *tub2*^{T238A}-induced microtubule hyperstabilization in terms of growth rate, cell size, DNA content, and spindle morphology. These results support the hypothesis that evolved *tub2*^{T238A} haploids recovered operational microtubules, which allowed regular cell cycle progression.

The earliest evolutionary response to microtubule hyperstabilization is aneuploidy, which is later replaced by point mutations in α - or β -tubulin.

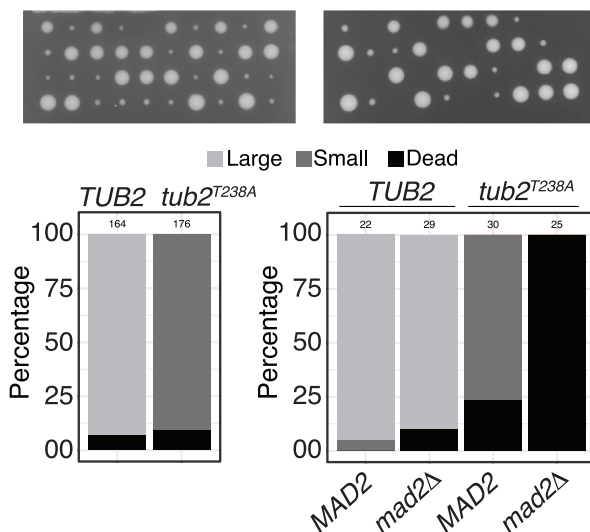
To identify the genetic changes underlying growth recovery, we obtained genome sequences for all populations at T1 and at Tf (Figure 1A); this provided for recurrent copy numbers of individual chromosomes and for mutation frequencies. To identify candidate compensatory mutations, we first screened for genes that were mutated in different residues in at least two different populations; we called them recurrently mutated genes (STAR Methods).

At T1, when the growth rate was still much decreased compared to the WT, no recurrently mutated genes were detected, but we observed recurrent aneuploidy, primarily for chromosomes XII and XVI and, to a lesser extent, for chromosomes IV, III, and IX (Figure 2A). Aneuploidy was not observed in WT cultures (Figure S2A). Because parental diploids also did not display recurrent aneuploidies (Figure S1B), these disomies were acquired before T1, sometime during the 5 days between sporulation and sequencing.

A



B



C

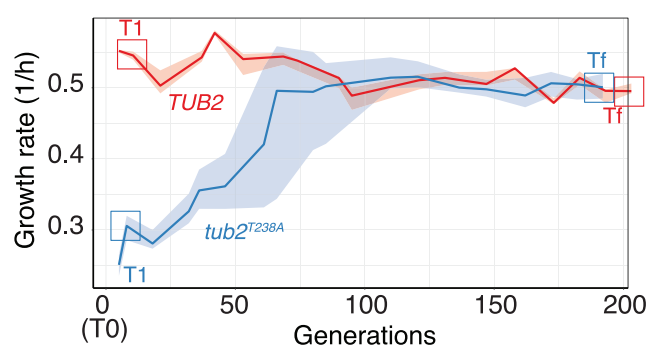


Figure 1. Laboratory evolution experiment with $tub2^{T238A}$ cells

(A) Schematic depicting the evolution experiment for $tub2^{T238A}$ and $TUB2$ cells. $TUB2/TUB2$ and $TUB2/tub2^{T238A}$ were sporulated, and single spores were grown on yeast extract peptone dextrose (YPD) plates. Based on marker selection, haploid cells were assigned as $TUB2::KanMX$ or $tub2^{T238A}::KanMX$. When colonies became visible, they were grown in liquid, and the growth rate was measured every 2 or 3 days until the end of the experiment.

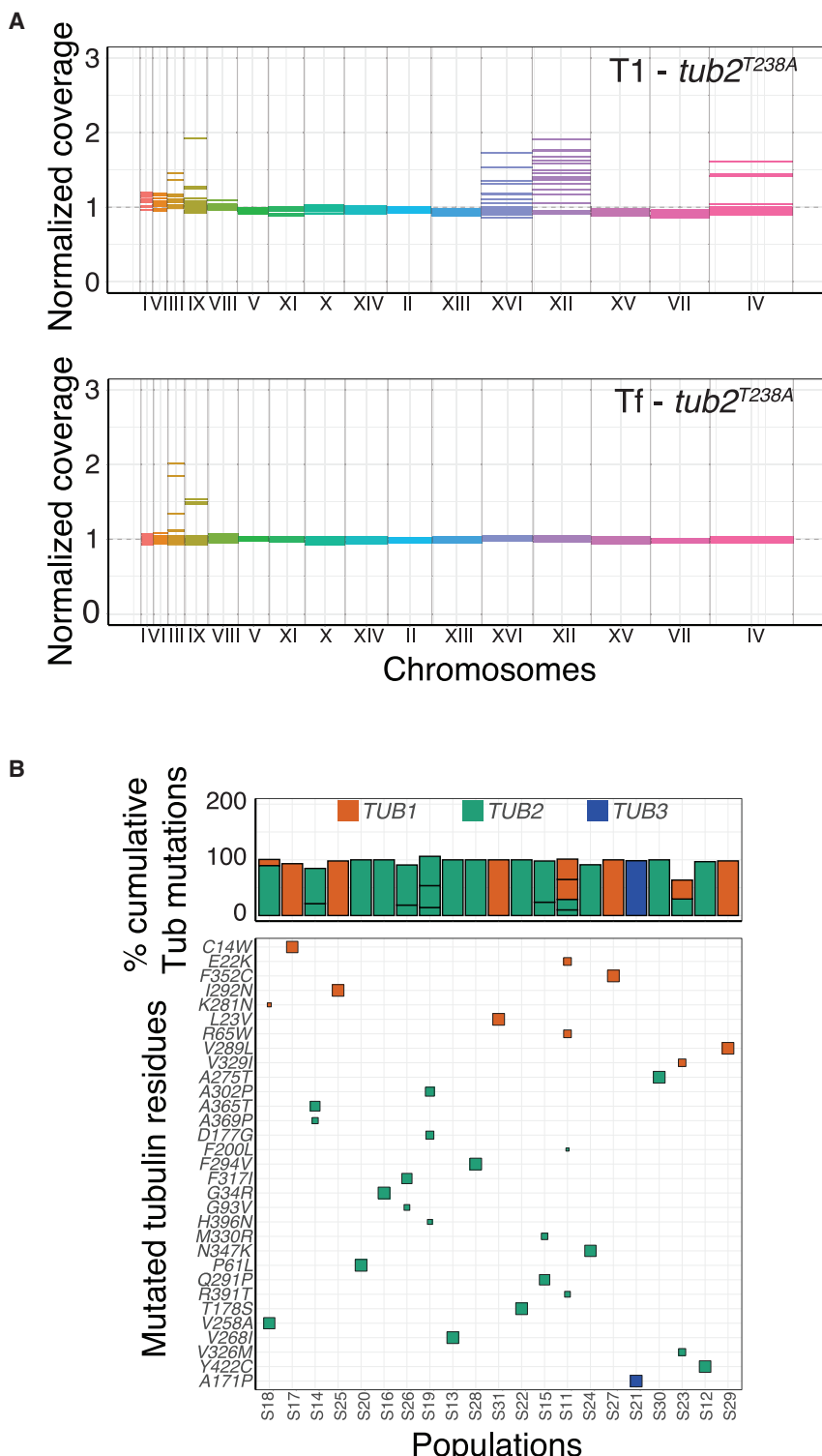
(B) Top: representative images of the haploid colonies obtained after 3 days from the dissection of $TUB2/tub2^{T238A}$ and $TUB2/tub2^{T238A} MAD2/mad2\Delta$ diploids. Bottom: relative fraction of large, small, or dead colonies. The numbers at the top of the bars represent the number of colonies analyzed for each genotype in 2 biological replicates.

(C) Growth rate measurements as a function of the number of generations, from the time cells were transferred to liquid medium to the end of the experiment. Thick lines mark the medians, and shadowed areas mark the interquartile ranges for the 5 WT and 21 $tub2^{T238A}$ evolved populations.

By contrast, at Tf, when growth was largely recovered, evolved $tub2^{T238A}$ cells showed mostly normal ploidy (Figure 2A). Only very few aneuploidies of chromosome III (chrIII) and chrIX were still visible. Instead, cells had acquired point mutations in the following recurrently mutated genes: $TUB1$, $TUB2$, $MCM21$, and $ERG24$ (Figure S2B, left). Among them, $TUB1$ and $TUB2$ were by far the most represented, and mutations in either of these two genes were detected in all evolved populations except one. In this specific population, however, we observed a mutation in $TUB3$, a gene that encodes a minor α -tubulin isoform in yeast. Hence, we also considered mutations affecting this gene as candidate compensatory mutations (Figure S2B, left).

None of the evolved populations reverted the $tub2^{T238A}$ mutation. We also noticed that no TUB mutation appeared in more than one population (Figure 2B). The summed frequency of TUB mutations in a population always approached but never exceeded 100% (Figure 2B, top). The simplest interpretation of this result is that in every population, the large majority of cells carry one, and no more than one, TUB mutation.

As for the two other recurrently mutated genes ($ERG24$ and $MCM21$), $ERG24$ mutations were present in two $tub2^{T238A}$ evolved populations at ~50% frequency (Figure S2B, left). $ERG24$, a gene involved in ergosterol biosynthesis, is not involved in microtubule-related processes. Moreover, a gene belonging to



the same ergosterol biosynthesis family (*ERG3*) was recurrently mutated in the WT evolved population together with *HAP1*, involved in the expression of *ERG* genes²⁶ (Figure S2B, right). This indicates that *ERG*-family mutations are likely independent

were capable of rescuing $tub2^{T238A}$ on their own. To choose a subset of mutations in different characteristic locations for intensive study, we examined the locations of tubulin mutations in the context of microtubule structure. Most of the mutations in

Figure 2. Genetic rearrangements in evolving cells

(A) Depth of coverage of $tub2^{T238A}$ at T1 and Tf. $tub2^{T238A}$ cells were collected for next generation sequencing (NGS) at T1 and Tf, and the normalized median coverage along each chromosome was analyzed as described in STAR Methods.

(B) Evolved tubulins mutations in $tub2^{T238A}$ cells at Tf (rows) in the different populations (columns). Top: cumulative frequency of mutations in the three tubulin genes for each population. Bottom: for each evolved population, we show specific mutations in tubulins. The dimension of the squares is proportional to the mutation frequency in the population.

from $tub2^{T238A}$, and so we did not include them as candidate $tub2^{T238A}$ compensatory mutations. Finally, *MCM21* mutations were observed in two populations. *Mcm21* is a component of the Ctf19/Okp1/Mcm21/Ame1 (COMA) complex, involved in regulation of the kineto-chore-mitotic spindle interaction during metaphase.^{27,28} Given its potential role in regulating microtubule-kinetochore attachment, and because it was not mutated in WT cultures, we took *MCM21* as a potential candidate for mutations compensating for the $tub2^{T238A}$ mutations. Thus, $tub2^{T238A}$ candidate compensatory mutations include those affecting *TUB1*, *TUB2*, *TUB3*, and *MCM21* (Figure S2B, left).

In summary, by sequencing populations at two different time points, we observed that specific disomies were selected first together with very limited recovery of growth. Eventually, when growth was consistently rescued, aneuploidies were largely replaced by point mutations. Among the latter, those affecting *TUB1*, *TUB2*, *TUB3*, and *MCM21* met our criteria to be $tub2^{T238A}$ candidate compensatory mutations.

Mutations in *TUB2* and *TUB1*, but not in *MCM21*, compensate for $tub2^{T238A}$

We first analyzed point mutations, the last and fittest evolutionary solutions. The most pervasive were mutations in tubulin genes. We tested whether they

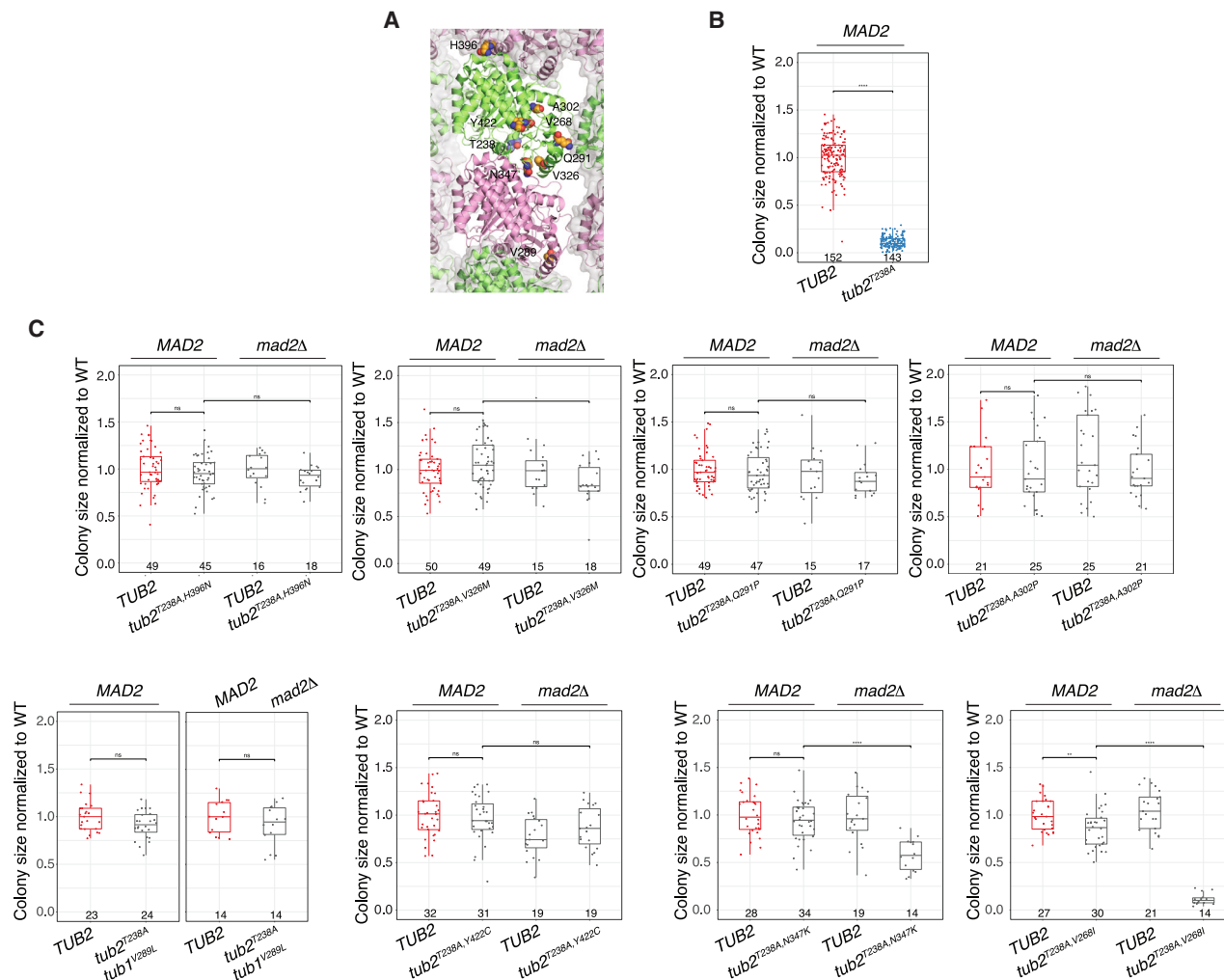


Figure 3. Evolved tubulin mutations compensate for the *tub2^{T238A}* mutation, and some rely on the mitotic checkpoint

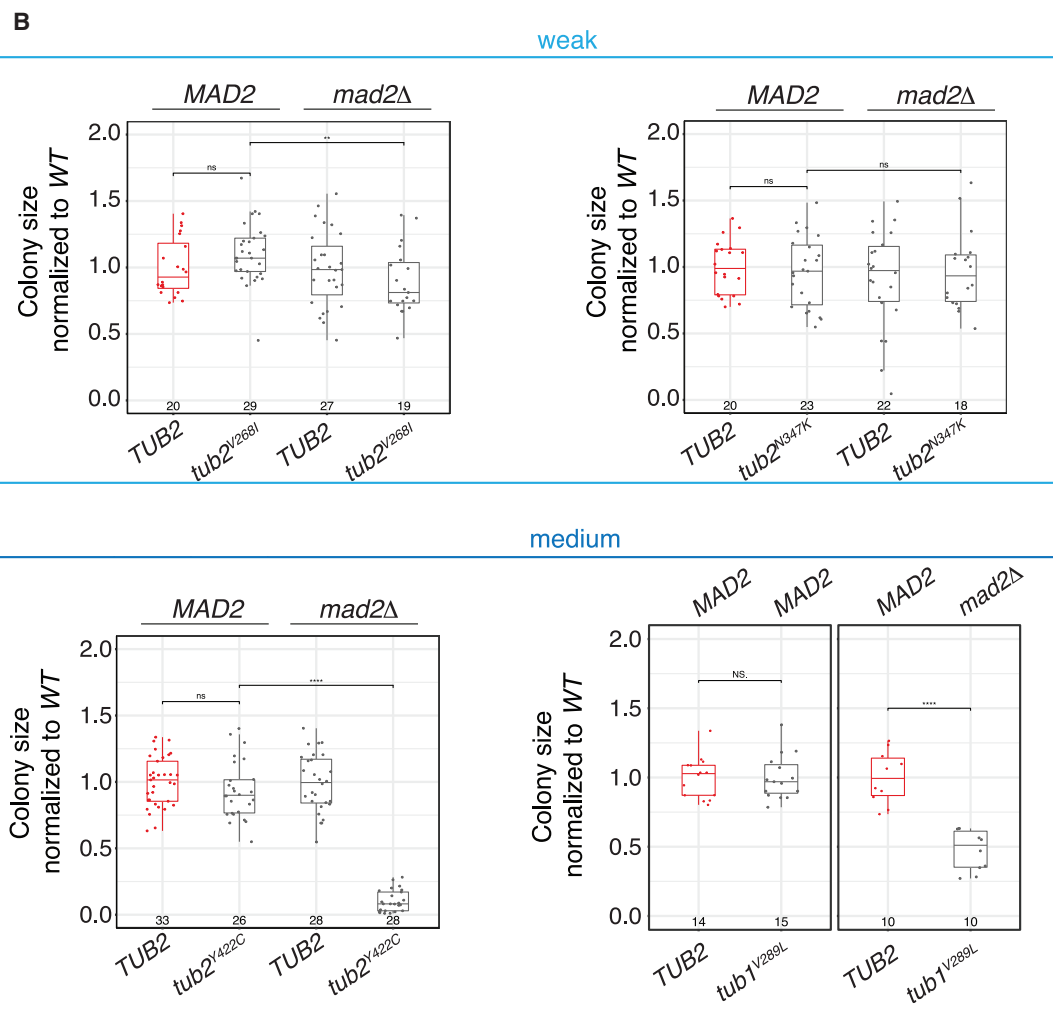
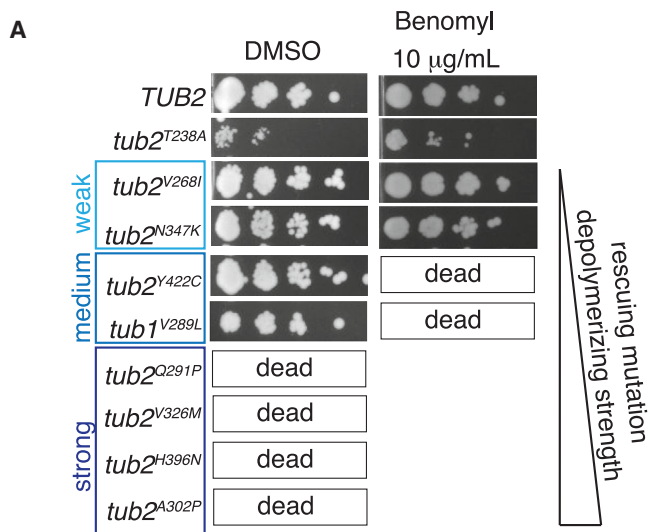
(A) Cartoon illustrating the positions of the subset of β -tubulin mutations chosen for more in-depth study. See Figure S3A for a representation showing all mutants. An $\alpha\beta$ -tubulin heterodimer (α , pink; β , green; PDB: F) is shown in the context of its microtubule neighbors (same coloring but with a translucent surface; PDB: 6O2R). The view is from the outside.

(B and C) Haploid colonies of the indicated genotypes obtained after 3 days from the dissection of the following diploids: (B) *TUB2/tub2^{T238A}* and (C) *TUB2/tub2^{T238A,H396N}* *MAD2/mad2* Δ, *TUB2/tub2^{T238A,V326M}* *MAD2/mad2* Δ, *TUB2/tub2^{T238A,Q291P}* *MAD2/mad2* Δ, *TUB2/tub2^{T238A,A302P}* *MAD2/mad2* Δ, *TUB2/tub2^{T238A}* *TUB1/tub1^{V289L}* *MAD2/mad2* Δ, *TUB2/tub2^{T238A,Y422C}* *MAD2/mad2* Δ, *TUB2/tub2^{T238A,N347K}* *MAD2/mad2* Δ, and *TUB2/tub2^{T238A,V268I}* *MAD2/mad2* Δ. For *tub1^{V289L}*, we used two different diploids, since *tub1^{V289L}* and *mad2* Δ have the same marker, which did not allow us to distinguish between *tub1^{V289L}* and *mad2* Δ. Sizes were normalized on the mean of the WT size. For each genotype, we indicate the number of colonies (N) measured in 2 biological replicates (n). Comparisons were made with a linear model (see STAR Methods for details) (ns, $p > 0.05$; * $p < 10^{-1}$; ** $p < 10^{-2}$; *** $p < 10^{-3}$; **** $p < 10^{-4}$).

both *TUB1* and *TUB2* were located on or near a microtubule lattice interface, or they were buried in the solvent-inaccessible core of the protein. By contrast, very few mutations were located on the outer surface of the microtubule (Figure S3A; Table S1). The subset of mutations we chose for more in-depth studies (Figure 3A) comprises *tub2^{H396N}* (at the longitudinal interface between tubulin dimers), *tub2^{N347K}* (at the longitudinal interface within tubulin dimers), *tub2^{V326M}* (buried inside the core of *TUB2*, on helix 10, which participates in the longitudinal interface within tubulin dimers), *tub2^{Q291P}* (at the lateral interface between tubulin dimers), *tub2^{V268I}* (buried inside the core of *TUB2*, close to the core helix on which *tub2^{T238A}* resides),

tub2^{Y422C} (buried inside the core of *TUB2*, near the C terminus of helix 12), *tub1^{V289L}* (partially buried and proximal to the longitudinal and lateral interface between tubulin dimers), and *tub2^{A302P}* (on the outer surface of the microtubule). We measured the growth of strains carrying these mutations in the presence of *tub2^{T238A}*. Growth assays confirmed that, unlike *tub2^{T238A}* (Figure 3B), they all rescued growth similarly as the WT (first two columns in Figure 3C), with only one mutation (*tub2^{T238A,V268I}*) showing a significant but minor decrease in growth.

To assess the ability of the selected mutations to rescue defects in chromosome segregation, we tested their growth in the absence



(legend on next page)

of *MAD2* (third and fourth column in [Figure 3C](#)). *tub2^{T238A,N347K}* and, even more markedly, *tub2^{T238A,V268I}* recovered growth only in the presence of *MAD2* (compare columns two and four in [Figure 3C](#)). The other mutants after *MAD2* deletion displayed growth comparable to the WT. All mutants, however, showed an euploid karyotype without recurrent aneuploidies ([Figure S3B](#)), implying that the mitotic checkpoint suffices to guarantee their genetic stability.

Finally, as for the role of *MCM21*, the colony size of *tub2^{T238A}* *mcm21^{E159D}* (E159D being the *MCM21* mutation with the highest frequency) was comparable to those of *tub2^{T238A}* alone ([Figure S3C](#)). This result implies that the *MCM21* mutation does not majorly compensate for *tub2^{T238A}*.

In summary, we identified representative mutations for tubulin genes based on their structural locations, and we showed that they all suffice to compensate for the *tub2^{T238A}* mutation. Growth of two mutants, *tub2^{T238A,V238I}* and *tub2^{T238A,N347K}*, relied on the mitotic checkpoint. The mutation in *MCM21*, instead, taken alone, did not have an obvious adaptive role.

***In vivo* analysis of compensatory tubulin mutations reveals differences among them**

To understand the different dependence on the mitotic checkpoint, we examined whether and how the mutations per se affected fitness in the absence of the T238A mutation. Four mutants, *tub2^{Q291P}*, *tub2^{V326M}*, *tub2^{H396N}*, and *tub2^{A302P}*, were not viable; we presume that they strongly compromise microtubule stability. The remaining mutations allowed for WT-like growth (left column in [Figure 4A](#) and first two columns in [Figure 4B](#)). To differentiate between these “weaker” mutations, we used as complementary assays both sensitivity to the microtubule destabilizing drug benomyl ([Figure 4A](#), right column) and synthetic interactions with *mad2Δ* (last two columns in [Figure 4B](#)). *tub1^{V289L}* and *tub2^{Y422C}* showed a growth defect when combined with *MAD2* deletion, a sign of increased chromosome mis-segregation likely caused by microtubule destabilization. Accordingly, these mutants were also sensitive to benomyl (right column in [Figure 4A](#)). *tub2^{N347K}* and *tub2^{V268I}* did not display a growth defect when combined with *MAD2* deletion, nor did they show enhanced sensitivity to benomyl (right column in [Figure 4A](#)). Thus, we ranked the microtubule-destabilizing activity of the compensatory mutations as follows: *tub2^{Q291P}*, *tub2^{V326M}*, *tub2^{H396N}*, and *tub2^{A302P}* (strong depolymerizers) > *tub2^{Y422C}* and *tub1^{V289L}* (medium depolymerizers) > *tub2^{N347K}* and *tub2^{V268I}* (weak depolymerizers). Noticeably, mutations of the last group relied on the mitotic checkpoint to rescue *tub2^{T238A}* ([Figure 3C](#)). The mutations yielding the strongest effect reside on or very near microtubule lattice contacts and may directly weaken tubulin:tubulin interactions.

***Figure 4. In vivo* analysis of the tubulin mutations**

- (A) Serial dilutions of *TUB2*, *tub2^{T238A}* cells, and cells carrying a subset of evolved mutations were spotted in YPD supplemented with DMSO or benomyl (10 μg/mL) at 30°. Images were taken after 2 days of growth. Number of replicates, *n* = 3.
- (B) Haploid colonies of the indicated genotypes obtained after 3 days after the dissection of the following diploids: *TUB2/tub2^{V268I}* *MAD2/mad2 Δ*, *TUB2/tub2^{N347K}* *MAD2/mad2 Δ*, *TUB2/tub2^{Y422C}* *MAD2/mad2 Δ*, *TUB1/tub1^{V289L}* (for *TUB2 MAD2* and *tub1^{V289L} MAD2*), and *TUB1/tub1^{V289L}* *MAD2/mad2 Δ* (for *MAD2 TUB2* and *mad2Δ tub1^{V289L}*). For *tub1^{V289L}*, we used two different diploids, since *tub1^{V289L}* and *mad2 Δ* have the same marker, which did not allow us to distinguish between *tub1^{V289L}* and *mad2Δ*. Sizes were normalized on the mean of the WT size. For each genotype, we indicate the number of colonies (*N*) measured in 2 biological replicates. Comparisons were made with a linear model (see [STAR Methods](#) for details) (ns, *p* > 0.05; ***p* < 10⁻²; ****p* < 10⁻⁴).

In summary, our data suggest that the various mutations may not restore microtubule stability to the same extent. We produced a ranking of depolymerizing strength for the rescuing *tub2* mutations that differentiates them in three classes, which we hypothesize to be strong, medium, and weak depolymerizers.

In vitro* analysis of compensatory tubulin mutations mirrors results obtained *in vivo

To confirm that compensatory mutations restore microtubule dynamics to different degrees, we measured *in vitro* the dynamics of microtubules carrying compensatory mutations together with the T238A mutation. We also reasoned that cells may not tolerate more than one compensatory mutation, which may explain why evolved cells carry one compensatory mutation of tubulin and not more than one ([Figure 2B](#), top). To test this idea, we explored the effect of combining two evolved mutations in the same *tub2^{T238A}*.

We focused on the same subset of *tub2* mutations that was described in the prior section ([Figure 4A](#), *tub2^{N347K}* was omitted for technical reasons). Mutations were introduced individually into the *tub2^{T238A}* expression construct and subsequently over-expressed and purified ([Figure S4A](#)).²⁹ The presence of all mutations was confirmed by intact mass spectrometry ([Table S2](#)).

When compared to the WT, and as reported previously,²³ *tub2^{T238A}* microtubules shrank over 100-fold more slowly and formed spontaneously (nucleated) at low concentrations at which WT microtubules did not. To compare the effect of different compensatory mutations on *tub2^{T238A}*, we focused on the shrinking rate because it is the most obvious proxy for microtubule (hyper)stability, and it can be compared across different concentrations of tubulin. The large magnitude difference between WT and *tub2^{T238A}* also provides a good dynamic range for rank-ordering the compensatory strength of different evolved mutations.

When combined with *tub2^{T238A}*, the mutations increased the shrinking rate compared to microtubules that contained *tub2^{T238A}* alone ([Figures 5A](#) and [5B](#)), indicating that they all restored more normal microtubule dynamics. The magnitude of the change varied widely; *tub2^{T238A,V326M}* microtubules shrank at a rate comparable to the WT. By contrast, *tub2^{T238A,V268I}* microtubules shrank only slightly faster than *tub2^{T238A}*. Consistent with this apparently weak effect, V268I was also the only compensatory mutation that did not increase the low threshold concentration for nucleation of *tub2^{T238A}*-containing microtubules (data not shown). Other evolved mutations showed intermediate degrees of compensation: Q291P and A302P compensated nearly completely, and H396N yielded weak compensation. Finally, Y422C gave partial compensation. In the case of this mutant, shrinkage was multi-phasic, and we measured the rate with

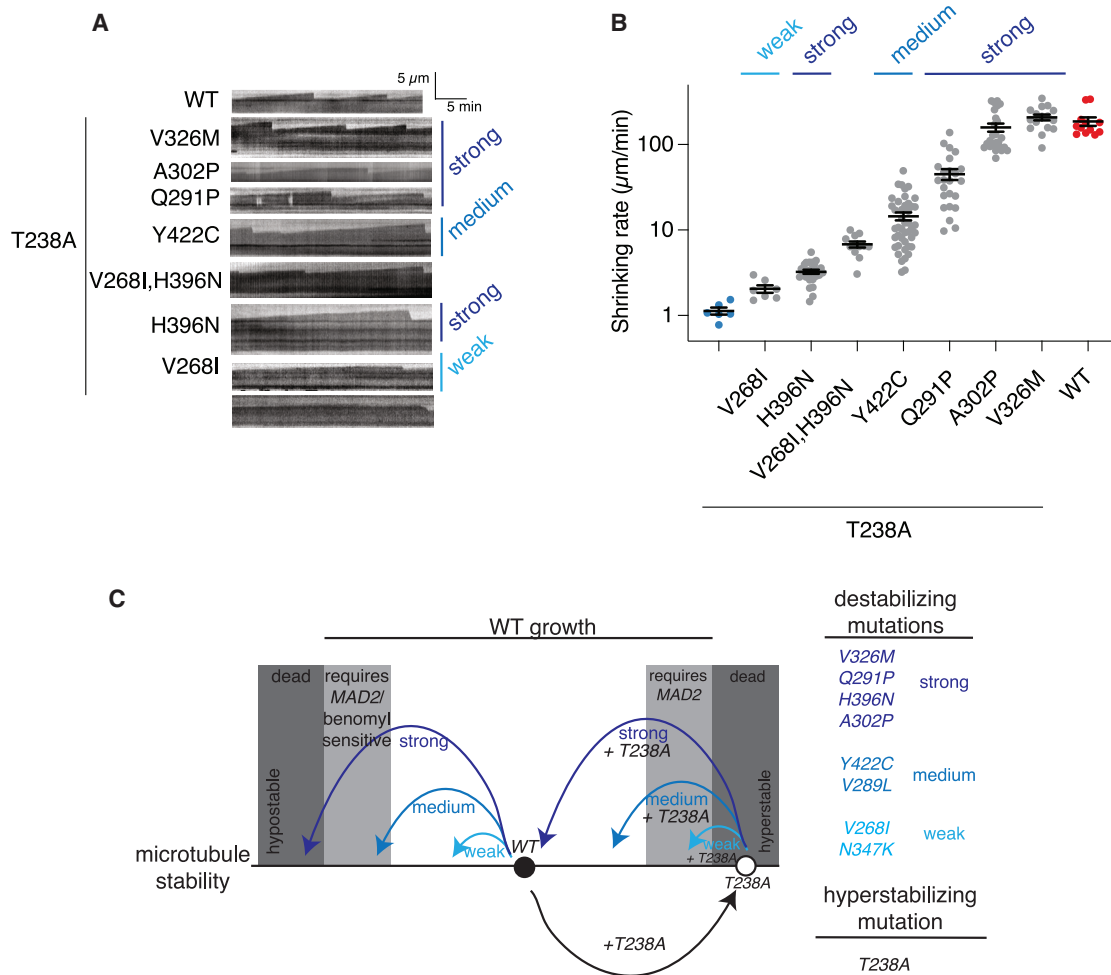


Figure 5. Evolved mutations restore microtubule dynamics to different degrees

(A) Representative kymographs showing polymerization dynamics for the indicated constructs. Labels indicate the mutations present in β -tubulin ($TUB2$); all samples contained WT α -tubulin ($TUB1$). Most measurements were performed at $0.3 \mu\text{M}$ concentration, but because of a greater tendency to spontaneously nucleate microtubules, T238A and T238A,V268I were measured at $0.08 \mu\text{M}$.

(B) Quantification of microtubule shrinking rates for the indicated constructs. $N = 6–44$ microtubules from at least two independent assays. Bars indicate mean and standard error of the mean.

(C) On the x axis, we plot microtubule stability and on the y axis growth. At the extremes of the plot, cells cannot grow due to excessive instability (left) or stability (right). Elsewhere, cells show WT growth. In the areas bordering excessive stability/instability, WT growth requires the mitotic checkpoint. The different rescue mutations, shown on the right, destabilize microtubules, while T238A hyperstabilizes them. The effect of weak, medium, and strong destabilizers is shown by the length of the arrows.

reduced time sampling (Figure S4B). Interestingly, the ranking we observed *in vitro* recapitulated the distinction in strong, medium, and weak destabilizers observed *in vivo*, with the only exception being $tub2^{H396N}$ for the shrinking rate (Table S3; Figure S4C).

Finally, the combination of V268I and H396N shrank faster than either individual mutation but much less than the best-performing mutations, showing that the simultaneous presence of two compensatory mutations does not disrupt microtubule dynamics (V268I and H396N in Figures 5A and 5B). This result can be explained by the fact that one compensatory mutation suffices to recover growth, and so additional mutations do not provide a strong selective advantage (diminishing return epistasis, see estimation of the expected number

of mutations in tubulin under STAR Methods and Figures S4D and S4E).

We summarized in Figure 5C the results obtained for the different mutants both *in vivo* (Figures 3 and 4) and *in vitro* (Figures 5A and 5B). The plot shows qualitatively the relation between growth and microtubule stability. The T238A mutation causes microtubule hyperstabilization, and the mutations we identified compensate for this to varying degrees. The schematic also shows how the dependency on the mitotic checkpoint and the effect of benomyl in the different mutants correlate well with the definition of weak, medium, and strong mutants.

We conclude that compensatory mutations rescue the hyperstabilizing T238A mutation by restoring shrinking rates. They do

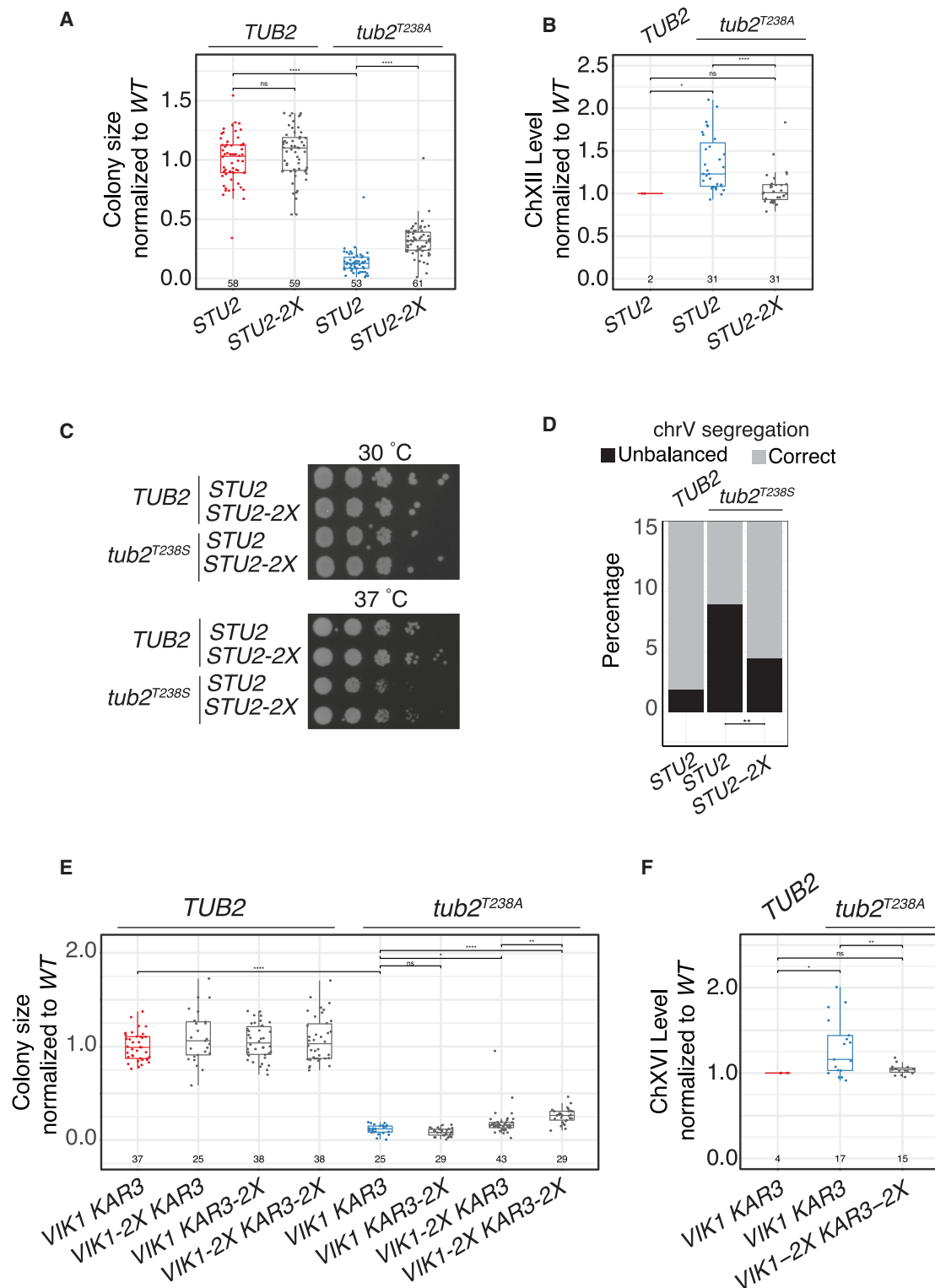


Figure 6. Rescues of growth observed upon the duplication of *STU2* and *VIK1/KAR3*

(A) Haploid colonies of the indicated genotypes were obtained after 3 days from the dissection of the *TUB2/tub2^{T238A}* *STU2/STU2-2X* diploid. Sizes were normalized on the mean of the WT size. For each genotype, we indicate at the bottom of the plots the number of colonies (N) measured in 2 biological replicates.

(legend continued on next page)

so to different degrees, largely recapitulating the rank ordering obtained from *in vivo* experiments in the absence of *MAD2*.

Increased dosage of *STU2*, a factor that regulates microtubule dynamics, accounts for the adaptive benefit of chrXII disomy

At T1, before tubulin mutations, we observed specific aneuploidies, primarily disomies of chrXII and chrXVI. We asked whether they could be explained by the increased dosage of proteins regulating microtubule dynamics.

STU2 (chTOG in humans), located on chrXII, codes for a microtubule polymerase that can promote microtubule depolymerization,^{30,31} and enhancement of this activity may explain the compensatory role of *STU2* duplication. Hence, we duplicated *STU2* (Figure S5A) and observed that *tub2^{T238A}* *STU2-2X* colonies were significantly bigger than *tub2^{T238A}* colonies but still smaller than WT colonies (Figure 6A). Moreover, after 48 h (i.e., at T1), genomic qPCR on chrXII showed that chrXII levels were significantly higher in *tub2^{T238A}* compared to WT cells, while *tub2^{T238A}* *STU2-2X* had values similar to the euploid WT (Figure 6B). This result shows that cells carrying two copies of *STU2* do not develop disomy of chrXII and implies that duplication of *STU2* underlies the observed disomy of evolved cells at an early time point. It is worth noting that evolved *tub2^{T238A}* likely has a consistent fraction of cells disomic for chrXII that also express *STU2* from two gene copies. Yet, *tub2^{T238A}* *STU2-2X* grew better, possibly because the duplication of other genes in chrXII disomic imposes a fitness cost that mitigates the benefits from increasing the dosage of *STU2*.

As noted earlier, residual viability of *tub2^{T238A}* requires the mitotic checkpoint (Figure 1B), implying that microtubule hyperstabilization caused by the mutation introduces errors in chromosome segregation. Hence, we asked whether *STU2* partially compensates for *tub2^{T238A}* by decreasing chromosome mis-segregation. Since *STU2-2X* *tub2^{T238A}* cells are strongly impaired in growth and are genetically unstable, we instead used *tub2^{T238S}*. This is a milder microtubule-hyperstabilizing mutation (Figure S5B)²³ that has a stronger phenotype at 37°C than at 30°C (Figure S5C), is also rescued by *STU2* duplication (Figure 6C), and allows conditional experiments directly in haploid cells. We followed the segregation of chrV-tagged GFP in *tub2^{T238S}*, and, in agreement with our hypothesis, we observed that the mis-segregation rate (**STAR Methods**) in *tub2^{T238S}* *STU2-2X* at 37°C was significantly lower than in *tub2^{T238S}* (but still higher than in the WT) (Figures 6D and S5D).

Thus, the recurrent disomy of chrXII can be explained by the increased dosage of *STU2*, which partially rescues the growth

defect and chromosome mis-segregation that accompany microtubule hyperstabilization.

Increased dosage of *VIK1/KAR3*, but not *IPL1*, accounts for the disomy of chrXVI

We then addressed the disomy of chrXVI, which was the second most frequent (Figure 2A). This chromosome carries *IPL1* (Aurora B in humans), which is a member of CPC and destabilizes erroneous microtubules/kinetochore attachment.^{16,32} We reasoned that increasing *Ipl1* activity may allow the use of hyperstabilized microtubules. However, *IPL1-2X* in *tub2^{T238A}* (Figure S6A) did not improve colony size (Figure S6B). The same was observed when we combined *IPL1-2X* with the duplications of *CTF19* and *MCM16* (Figures S6A and S6B), two components of the COMA complex²⁸ also present on chrXVI. To test whether *Ipl1* was at least necessary for the rescue effect, we deleted one endogenous allele of *IPL1* in the *TUB2/tub2^{T238A}* diploid and inserted a copy of *IPL1* on chrIII. We then repeated the evolution experiment and observed that, at T1, disomy of chrXVI showed a similar frequency regardless of whether *IPL1* was located on chrIII or chrXVI. Additionally, the disomy of chrIII was not increased (Figure S6C). We conclude that *IPL1* duplication is neither necessary nor sufficient for the disomy of chr XVI.

Among other potential candidates on chrXVI, we considered *Irc15*, a microtubule-associated protein whose deletion decreases microtubule dynamics³³; *Kar9*, whose overexpression has been associated with increased benomyl sensitivity^{34,35}; and *Vik1*, which, in complex with *Kar3*, induces microtubule catastrophes in mitosis.³⁶ Duplicating *IRC15* or *KAR9* (Figure S6D) did not improve fitness (Figure S6E). However, when we produced *tub2^{T238A}* *VIK1-2X* (Figure S6A), we did observe improved growth, especially in the double mutant *tub2^{T238A}* *VIK1-2X* *KAR3-2X* (Figure 6E). Confirming that their duplication underlies the disomy, we also observed a sharp decrease in disomy of chrXVI in the haploids expressing two copies of *VIK1* and *KAR3* (Figure 6F).

In summary, our results show that duplication of *VIK1* and *KAR3*, which code for proteins reported to increase microtubule dynamics, underlies the disomy of chrXVI; *Ipl1*, instead, does not play a relevant role.

Tubulin mutations are generated independent of aneuploidies

Finally, we investigated the interplay between compensatory mutations and aneuploidy. The evolutionary dynamics can be visualized in a plot where we include four populations, all of them

(B) Haploid colonies of the indicated genotypes were obtained after 3 days from the dissection of the *TUB2/tub2^{T238A}* *STU2/STU2-2X* diploid and grown in liquid for 48 h, and then the levels of the right arm of chrXII were assessed by qPCR and normalized to the WT. The numbers at the bottom of the plots represent the number (N) of colonies analyzed for each genotype in 2 biological replicates.

(C) Serial dilutions of the indicated strains were spotted in YPD at 30°C or 37°C. Images were taken after 2 days of growth. n = 3.

(D) Percentage of mis-segregation events in WT and *tub2^{T238S}* cells with or without *STU2* duplication. Cells carrying GFP-tagged chrV were synchronized in α-factor at 30°C and released at 37°C. Images were collected 90 min after release. n = 4.

(E) Haploid colonies of the indicated genotypes were obtained 3 days after dissection of the *TUB2/tub2^{T238A}* *VIK1/VIK1-2X* *KAR3/KAR3-2X* diploid. Sizes were normalized on the mean of the WT size. For each genotype, we indicate at the bottom of the plots the number of colonies (N) measured in 2 biological replicates.

(F) Haploid colonies of the indicated genotypes were obtained 3 days after the dissection of the *TUB2/tub2^{T238A}* *VIK1/VIK1-2X* *KAR3/KAR3-2X* diploid and grown in liquid for 48 h, and then the left arm of chrXVI levels were assessed by qPCR and normalized to the WT. The numbers at the bottom of the plots represent the number (N) of colonies analyzed for each genotype in 2 biological replicates. Comparisons were made with a linear model (see **STAR Methods** for details) (ns, p > 0.05; *p < 10⁻¹; **p < 10⁻²; ***p < 10⁻³; ****p < 10⁻⁴).

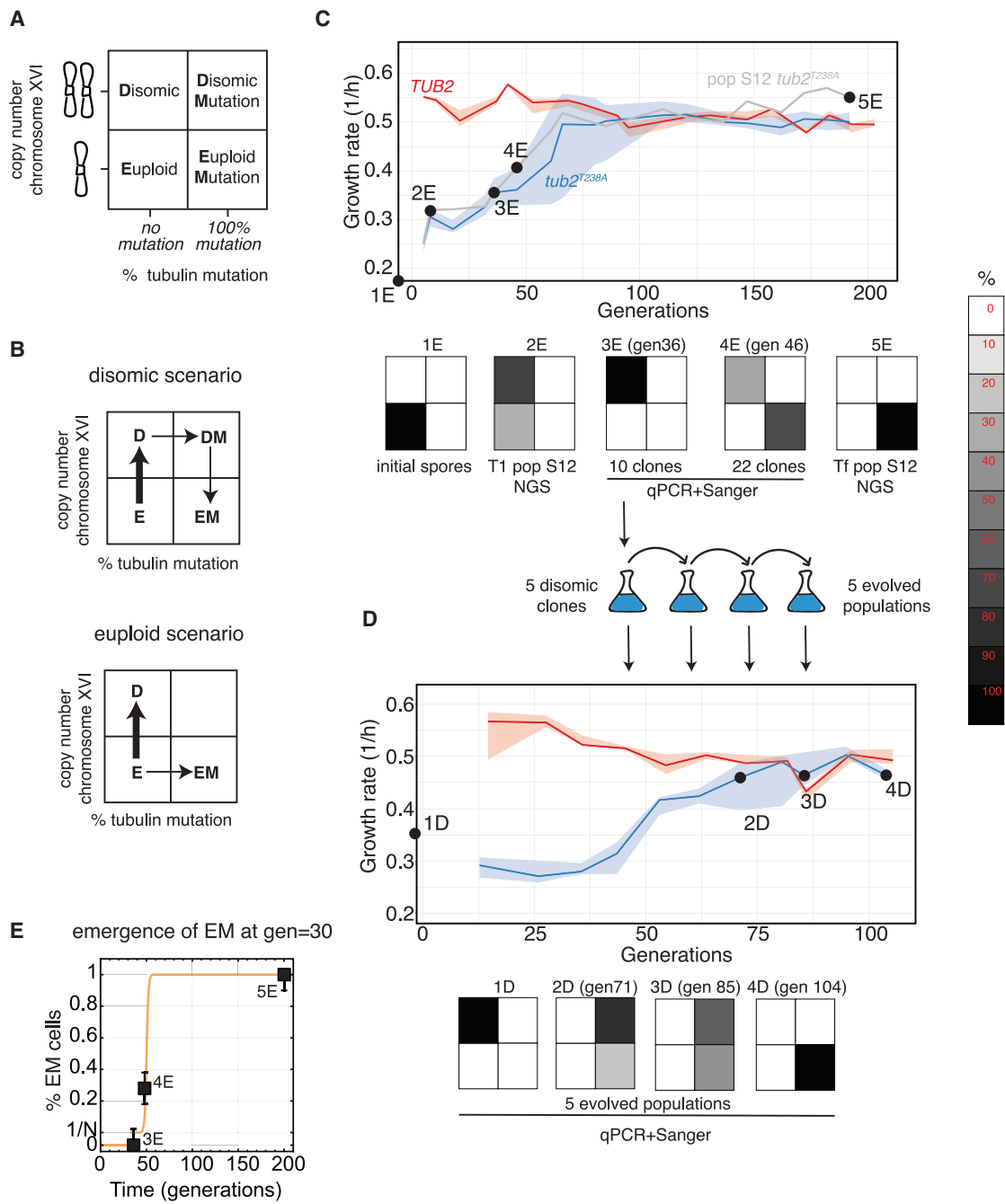


Figure 7. Disomic and euploid scenarios for the generation of resistant euploid cells

(A) During compensatory evolution, euploid cells can change ploidy (up/down) or acquire compensatory tubulin mutations (left/right). For each box, we identify the different sub-population (E, euploid; D, disomic; EM, euploid with mutation; DM, disomic with mutation).

(B) In the evolution experiment, cells start from E and end up being EM. EM cells can either be formed from DM cells (top, disomic scenario) or from E cells (bottom, euploid scenario). The thick vertical line represents the increased mis-segregation rate coming with the $T238A$ mutation.

(C) Growth rate dynamics of one specific population (S12) are superimposed on the WT and $tub2^{T238A}$ trajectories already shown in Figure 1C. Growth rate was measured every 2 or 3 days until the end of the experiment. The shaded boxes display the frequencies of the populations depicted in (A) at the different time points indicated in the growth rate dynamics. The different frequencies were measured as follows. The genetic background of initial spores was genetically determined (Figure 1A). T1 and Tf were determined by NGS on the whole population. For generations 36 and 46, we performed qPCR and Sanger sequencing of the tubulin gene on individual clones (Figures S7A and S7B).

(legend continued on next page)

carrying $tub2^{T238A}$ (Figure 7A): euploids (E), disomics (D), disomics with compensatory tubulin mutation (DM), and euploids with compensatory tubulin mutation (EM). At the population level, the normalized chromosome value measured by qPCR can take non-integer values. For the sake of simplicity, we set a threshold of 1.5 to define populations as D (>1.5) or E (<1.5).

In the experiment, we observed cells going from E (initial spores) to EM (at Tf). This can happen either directly or indirectly via the loss of disomy from DM (Figure 7B). We call the first possibility the “euploid scenario” and the second the “disomic scenario.” To distinguish between them, we derived clones from a $tub2^{T238A}$ population (S12) that showed high frequency (~70%) of chrXVI disomy at T1 (Figure S7A) and the mutation Y422C on *TUB2* with a frequency of 100% at Tf (Figure 2B). We isolated 10 clones from the population at generation 36 and 22 clones at generation 46. We measured the frequency of the Y422C mutation (by Sanger sequencing) and disomy (by qPCR; Figure S7B) and observed that all clones were D at generation 36. Ten generations later, of 22 clones, 7 were D, and 15 were EM with the mutation at 100% frequency. None were either DM or E. These results show that population D is almost completely replaced by EM in only 10 generations (Figure 7C). Yet, based on these data, we could not discriminate whether the compensatory mutation originated from DM, by loss of the extra chromosome, or E cells, by acquisition of the mutation.

To understand whether the disomic scenario is possible, we started a new evolution experiment with 5 populations originated from D clones (Figure 7D). They were analyzed by Sanger sequencing and qPCR (Figure S7C) at three time points, spaced by ~15 generations. At the first time point, we found that four populations were DM and one EM. After ~15 generations, the level of disomy decreased slightly, and finally, after another ~15 generations, all populations became EM. Importantly, the same mutations detected in DM were then identified in the EM populations. This result shows that the disomic scenario is possible. However, its dynamics are much slower than what was observed in the original experiment, which leads us to think that it cannot explain the dynamics observed in population S12 (Figure 7C).

The alternative euploid scenario assumes that (1) at least one EM cell was present around generation 30 and (2) that this was sufficient to explain the dynamics of population S12 (Figure 7C). To address this last point, we measured growth rates of disomic and euploid mutated cells (Figure S7D). With a mathematical model (see [mathematical modeling of the euploid scenario](#) under [STAR Methods](#)), we show that the observed dynamics can be recapitulated simply by assuming a competition between D and EM cells (Figure 7E). With the model, we also show that, given the measured growth rates, population size, and published mutation rate, we can expect the emergence of EM cells from the

sub-population of euploid cells around generation 30. This result shows that, unlike the disomic scenario, the euploid scenario is consistent with available data.

In conclusion, our data suggest that $tub2^{T238A}$ cells that acquire compensatory mutations do not originate from disomic cells but directly from $tub2^{T238A}$ euploids.

DISCUSSION

We performed an evolution experiment to determine how cells adapt to hyperstable microtubules. We used a well-characterized point mutation in the solvent-inaccessible core of β -tubulin, T238A, to perturb microtubule stability with high selectivity. We identified two types of temporally distinct and mutually exclusive genetic changes: point mutations in tubulin, which provide strong rescue, and disomies, which have a more limited response.

A role of checkpoint controls in adaptive evolution

Our results show a role of the mitotic checkpoint in supporting chromosome segregation for tubulin mutations less efficient in restoring microtubule dynamics. Different rescue efficiencies were evident and similar in experiments performed *in vitro* and *in vivo*, which led us to classify mutants as weak, medium, and strong depolymerizers.

One may hypothesize that weaker destabilizers make mistakes during chromosome attachment, which may be fixed thanks to the mitotic checkpoint. This is indeed what we found; all mutants rescued growth of $tub2^{T238A}$, including the weakest mutation, $tub2^{T238A,V268I}$. However, in the case of weak depolymerizers ($tub2^{T238A,V268I}$ and $tub2^{T238A,N347K}$), growth was reduced drastically after *MAD2* deletion (first two columns in Figure 3C; all data are summarized in Table S3 and Figure 5C). The role of the mitotic checkpoint was further confirmed by following the cell cycle dynamics of one weak and one strong depolymerizer: *V268I* and *Q291P*, respectively. The former spent a longer time with a G2 peak (i.e., in mitosis) than the latter, which behaved like the WT (Figures S7E and S7F). Accordingly, nuclear division was delayed by the same amount of time (data not shown). In summary, these data show that, without the mitotic checkpoint, weak depolymerizers would have been outcompeted and not selected in our evolution experiment.

Generalizing our results, we propose that the mitotic checkpoint may play a relevant role in adaptive evolution to mitotic defects. It does not belong to the target genes whose mutation compensates for the original fitness defect. However, it increases the target size, enlarging the ensemble of compensatory mutations and, thus, potentially accelerating adaptive evolution.

(D) Five clones taken from generation 36 of population S12 were evolved in liquid; the growth rate was measured every 2 or 3 days until the end of the experiment. In the shaded boxes, we show the frequencies of the populations depicted in (A) at the different time points. Frequencies of subpopulations were determined via qPCR and Sanger sequencing of tubulin genes on the 5 populations (Figure S7C).

(E) Mathematical model prediction of the EM population dynamics under the assumption that one EM cell is generated at generation 30 from E cells and competes with D cells. The growth rate of EM and D cells is shown in Figure S7D. The growth rate of E is estimated to be ~0.16 given the growth rate population at T0–T1 in Figure 1A and the fraction of aneuploid cells from Figure S7A. Population size is assumed to be ~ 10^7 from OD measurements and the mutation rate 1.7×10^{-10} (Zhu et al.³⁷). Details of the mathematical modeling are given in [mathematical modeling of the euploid scenario](#) under [STAR Methods](#).

Compensatory mutations arise independent of aneuploidy

In several evolution-repair experiments, aneuploidy has been identified first, followed by point mutations.^{6,8,9} Following the original interpretation,⁸ these data have been explained with the quick and costly repair due to aneuploidy, which is then replaced by less likely but more efficient compensatory mutations. However, theoretical modeling suggests that this may not always be the case; compensatory mutations can arise from euploid cells before aneuploids fully fix the population, allowing the mutations to then outcompete the aneuploids.³⁸ Along the same line, the original result⁸ has been re-interpreted, arguing that aneuploidy may not be a step toward adaptive evolution but, rather, a diversion.¹¹ Our experimental data show that, in our system, this is indeed the case. This result, however, depends on the specific experimental conditions. Simply changing the initial frequency of disomic cells, we channeled adaptive evolution toward a path where compensatory mutations are first observed in aneuploid cells. In conclusion, while aneuploidy is a widespread solution for cells that adapt to stressful conditions, its actual role needs to be examined case by case.

Only tubulin mutations rescue the hyperstabilizing T238A mutation

Our results extend a prior study of ours that investigated how cells evolve when microtubules are destabilized,⁹ wherein we also observed pervasive tubulin mutations. However, when there was a lack of microtubules, mutations restoring their polymerization were not a surprise, since cells cannot survive without microtubules. In the present case, we initially hypothesized that cells may be able to optimize the use of stabilized microtubules by leveraging the CPC protein Ipl1. However, our data clearly demonstrate that Ipl1 is neither necessary nor sufficient to explain the disomy of chrXVI. Instead, all mutations we found were in tubulins. Regardless of their position in the microtubule lattice, all mutations we tested *in vitro* (even that located on the surface of the polymers) restored the microtubule shrinking rate.

Why do tubulins show such a unique and limited genetic landscape of compensatory mutations? Other experiments that resulted in multiple types of compensatory mutations started with gene deletions, whereas here, we start from a point mutation. Consequently, and in contrast to our study, in these other evolution-repair experiments, second-site mutations that restore the original functionality of the impaired genes were not a possible outcome. However, this difference does not explain why, in our experiments, we did not observe mutations in other modules (e.g., CPC, anaphase promoting complex/cyclosome) which were mutated in response to other insults that affected chromosome segregation.^{6,39} One possibility is that structural components such as microtubules need to be restored to their original form or invented again⁷.

In agreement with this idea, we observed that restoration of microtubule dynamics can also explain the two main disomies we observed. The dosage increase in Stu2 on chrXII and Vik1 and Kar on chrXVI is responsible for the adaptive role of these disomies. Stu2 can alter microtubule growing and shrinking rates and has a mitotic role at kinetochores to control microtubule

turnover rate.^{40–42} The Vik1:Kar3 complex can increase the rate of microtubule catastrophe.³⁶

Finally, we note that, if our hypothesis is correct, then similar restoration-of-function mutations should also be pervasive when other “structural” components are affected; for example, actin.

Mutations in patients

Our results are not only relevant in the context of evolution experiments but could also be important for understanding the emergence of resistance in patients treated with microtubule-targeting drugs. The mammalian homolog of Stu2, chTOG, is overexpressed in a variety of tumors.^{43,44} Kar3 is a kinesin-14 motor, and overexpression of the human kinesin-14 KIFC1 and KIFC3 has been associated with resistance to taxane treatment.⁴⁵ As for the tubulin mutations, several residues mutated in cancer patients (some treated with taxanes and others not; <https://tubulinmutations.bio.uci.edu/>) were also mutated in the evolution experiments. In particular, some mutations (*tub1*^{E22K}, *tub2*^{Y422C}, *tub2*^{D177G}, and *tub2*^{T178A}) were selected in mammalian cell lines, including cancer cells, in response to the microtubule hyperstabilizing drugs paclitaxel and epothilone.^{46–48} Other mutations (*tub2*^{D177G}, *tub2*^{A275T}, *tub2*^{A365S}, and *tub2*^{Q291R}) were also found in the β-tubulin isotypes of breast cancer patients.⁴⁹ Finally, almost all *TUB2* mutations found in our yeast evolution experiment were in residues conserved in humans, and the overlap between residues mutated in the evolution experiment and in cancer patients is statistically significant ($p = 0.002$, see [overlapping between compensatory mutations and those detected in in patients under STAR Methods](#)). In this light, the observation that the mitotic checkpoint becomes essential for some rescuing mutations indicates a possible therapeutic possibility for selectively targeting cells that have become resistant to microtubule-targeting drugs via tubulin mutations. Finally, we propose that our experimental system can be used to predict mutations that may provide resistance to treatment with taxanes and, likewise, to assign to patients' mutations a possible role in the resistance to treatment.

Limitations of the study

Our work came with some limitations. First, we could only indirectly determine the route that cells follow to resistance, via mathematical modeling based on mutation frequencies of a limited number of populations. Hence, the hypothesis we propose is the most likely, but we could not provide direct evidence of aneuploidy being a diversion toward resistance. A second limitation of this study comes from the lack of a permissive condition for the *tub2*^{T238A} mutant. As a consequence, we could not perform in-depth characterization of the mutation in terms of cell biology (e.g., single-cell analysis showing chromosome dynamics after the mutation is expressed).

To conclude, our study showed that cells can rescue microtubule hyperstabilization. To do so, they have to recover microtubule dynamics. This, even to a minimal degree, is sufficient to fully recover growth thanks to the presence of an operational mitotic checkpoint. It will be important in the future to confirm the generality of these conclusions for other structural components.

RESOURCE AVAILABILITY

Lead contact

Further information and requests for resources and reagents should be directed to and will be fulfilled by the lead contact, Andrea Ciliberto (andrea.ciliberto@ifom.eu).

Materials availability

Materials generated in this study (e.g., yeast strains) are available upon material transfer agreement (MTA) completion and upon request from the [lead contact](#).

Data and code availability

- NGS data have been deposited at EBI-EMBL Array Express-BioStudies and are publicly available as of the date of publication. The accession number is listed in the [key resources table](#).
- This paper does not report original code.
- Any additional information required to reanalyze the data reported in this paper is available from the [lead contact](#) upon request.

ACKNOWLEDGMENTS

We thank Marco Cosentino Lagomarsino for support and discussions throughout the development of this project and Silke Hauf and Andrea Musacchio for comments on the manuscript. For financial support, F.M. benefited from an Italian Association of Cancer Research (AIRC) fellowship while she was a PhD student at the University of Galway. S.P. is the recipient of an FUV fellowship. T.B. is supported by the NIH molecular biophysics training grant T32GM131963. Research in the A.C. lab is financed by the Italian Association for Cancer Research (AIRC) (IG-28821), by donations from the Suma-Nesi family, and by the Hungarian National Research, Development and Innovation Office through grant TKP2021-EGA-42. The L.M.R. lab is supported by the NIH (R01-GM098543) and the NSF (MCB-2017687). F.G. receives funding from the French National Research Agency (ANR; JCJC grant ANR-23-CE54-0009-01). We thank G. Rancati for the gift of oligos for karyotyping.

AUTHOR CONTRIBUTIONS

F.M. designed, analyzed, and performed all experiments except for those shown in **Figures 5A** and **5B**, which were produced by T.B. and J.C.A. under the supervision of L.M.R., and those shown in **Figures S7E–S7F**, produced by P.B. and E.C. F.G. and P.B. contributed extensively to the analysis of NGS data. P.B. and E.C. contributed to the design of the evolution experiment and data analysis. S.P. did the mathematical analyses in **STAR Methods**, and F.G. analyzed the overlapping of evolved mutations with those identified in patients. A.C. obtained financial support, designed the experiments, and supervised the project. A.C. wrote the text with extensive contributions from L.R. and F.M.

DECLARATION OF INTERESTS

The authors declare no competing interests.

STAR METHODS

Detailed methods are provided in the online version of this paper and include the following:

- [KEY RESOURCES TABLE](#)
- [EXPERIMENTAL MODEL AND STUDY PARTICIPANT DETAILS](#)
 - Media and growth conditions
- [METHOD DETAILS](#)
 - Evolution experiment
 - Liquid growth assay
 - Drop test assay
 - Colony size analysis
 - Tubulin immunofluorescence

- Flow cytometry for apparent ploidy/DNA content
- Flow cytometry for cell size
- Sanger sequencing of selected genes
- Evaluation of mis-segregation
- DNA extraction
- Genomic qPCR on chrXII and chrXVI
- Genomic qPCR on selected genes
- Sequencing and bam files creation
- Analysis of aneuploidy
- Cumulative ploidy
- Identification of single-nucleotide variants and short indels
- Identification of candidate mutations and recurrently mutated genes

● QUANTIFICATION AND STATISTICAL ANALYSIS

● ADDITIONAL RESOURCES

- Estimation of the expected number of mutations in tubulin
- Mathematical modeling of the euploid scenario
- Overlapping between compensatory mutations and those detected in patients

SUPPLEMENTAL INFORMATION

Supplemental information can be found online at <https://doi.org/10.1016/j.celrep.2025.115323>.

Received: June 26, 2024

Revised: November 15, 2024

Accepted: January 27, 2025

Published: February 15, 2025

REFERENCES

1. LaBar, T., Phoebe Hsieh, Y.Y., Fumasoni, M., and Murray, A.W. (2020). Evolutionary Repair Experiments as a Window to the Molecular Diversity of Life. *Curr. Biol.* 30, R565–R574. <https://doi.org/10.1016/j.cub.2020.03.046>.
2. Szamecz, B., Boross, G., Kalapis, D., Kovács, K., Fekete, G., Farkas, Z., Lázár, V., Hrtyan, M., Kemmeren, P., Groot Koerkamp, M.J.A., et al. (2014). The genomic landscape of compensatory evolution. *PLoS Biol.* 12, e1001935. <https://doi.org/10.1371/journal.pbio.1001935>.
3. Fumasoni, M., and Murray, A.W. (2020). The evolutionary plasticity of chromosome metabolism allows adaptation to constitutive DNA replication stress. *Elife* 9, e51963. <https://doi.org/10.7554/eLife.51963>.
4. Fumasoni, M., and Murray, A.W. (2021). Ploidy and recombination proficiency shape the evolutionary adaptation to constitutive DNA replication stress. *PLoS Genet.* 17, e1009875. <https://doi.org/10.1371/journal.pgen.1009875>.
5. Laan, L., Koschwanetz, J.H., and Murray, A.W. (2015). Evolutionary adaptation after crippling cell polarization follows reproducible trajectories. *Elife* 4, e09638. <https://doi.org/10.7554/eLife.09638>.
6. Clarke, M.N., Marsoner, T., Adell, M.A.Y., Ravichandran, M.C., and Campbell, C.S. (2023). Adaptation to high rates of chromosomal instability and aneuploidy through multiple pathways in budding yeast. *EMBO J.* 42, e111500. <https://doi.org/10.15252/embj.2022111500>.
7. Rancati, G., Pavelka, N., Fleharty, B., Noll, A., Trimble, R., Walton, K., Perera, A., Staehling-Hampton, K., Seidel, C.W., and Li, R. (2008). Aneuploidy underlies rapid adaptive evolution of yeast cells deprived of a conserved cytokinesis motor. *Cell* 135, 879–893. <https://doi.org/10.1016/j.cell.2008.09.039>.
8. Yona, A.H., Manor, Y.S., Herbst, R.H., Romano, G.H., Mitchell, A., Kupiec, M., Pilpel, Y., and Dahan, O. (2012). Chromosomal duplication is a transient evolutionary solution to stress. *Proc. Natl. Acad. Sci. USA* 109, 21010–21015. <https://doi.org/10.1073/pnas.1211150109>.
9. Pavani, M., Bonaiuti, P., Chirolí, E., Gross, F., Natali, F., Macaluso, F., Póti, Á., Pasqualato, S., Farkas, Z., Pompei, S., et al. (2021). Epistasis,

- aneuploidy, and functional mutations underlie evolution of resistance to induced microtubule depolymerization. *EMBO J.* 40, e108225. <https://doi.org/10.15252/embj.2021108225>.
10. Ravichandran, M.C., Fink, S., Clarke, M.N., Hofer, F.C., and Campbell, C.S. (2018). Genetic interactions between specific chromosome copy number alterations dictate complex aneuploidy patterns. *Genes Dev.* 32, 1485–1498. <https://doi.org/10.1101/gad.319400.118>.
 11. Kohanovski, I., Pontz, M., Vande Zande, P., Selmecki, A., Dahan, O., Pilpel, Y., Yona, A.H., and Ram, Y. (2024). Aneuploidy Can Be an Evolutionary Diversion on the Path to Adaptation. *Mol. Biol. Evol.* 41, msae052. <https://doi.org/10.1093/molbev/msae052>.
 12. Hughes, D., and Andersson, D.I. (2015). Evolutionary consequences of drug resistance: shared principles across diverse targets and organisms. *Nat. Rev. Genet.* 16, 459–471. <https://doi.org/10.1038/nrg3922>.
 13. Desai, A., and Mitchison, T.J. (1997). Microtubule polymerization dynamics. *Annu. Rev. Cell Dev. Biol.* 13, 83–117. <https://doi.org/10.1146/annurev.cellbio.13.1.83>.
 14. Bakhour, S.F., Genovese, G., and Compton, D.A. (2009). Deviant kinetochore microtubule dynamics underlie chromosomal instability. *Curr. Biol.* 19, 1937–1942. <https://doi.org/10.1016/j.cub.2009.09.055>.
 15. Bakhour, S.F., Thompson, S.L., Manning, A.L., and Compton, D.A. (2009). Genome stability is ensured by temporal control of kinetochore-microtubule dynamics. *Nat. Cell Biol.* 11, 27–35. <https://doi.org/10.1038/ncb1809>.
 16. Carmena, M., Wheelock, M., Funabiki, H., and Earnshaw, W.C. (2012). The chromosomal passenger complex (CPC): from easy rider to the godfather of mitosis. *Nat. Rev. Mol. Cell Biol.* 13, 789–803. <https://doi.org/10.1038/nrm3474>.
 17. Lara-Gonzalez, P., Pines, J., and Desai, A. (2021). Spindle assembly checkpoint activation and silencing at kinetochores. *Semin. Cell Dev. Biol.* 117, 86–98. <https://doi.org/10.1016/j.semcdb.2021.06.009>.
 18. Yang, C.P.H., and Horwitz, S.B. (2017). Taxol(R): The First Microtubule Stabilizing Agent. *Int. J. Mol. Sci.* 18, 1733. <https://doi.org/10.3390/ijms18081733>.
 19. Waters, J.C., Chen, R.H., Murray, A.W., and Salmon, E.D. (1998). Localization of Mad2 to kinetochores depends on microtubule attachment, not tension. *J. Cell Biol.* 141, 1181–1191. <https://doi.org/10.1083/jcb.141.5.1181>.
 20. Zhou, A.S., Tucker, J.B., Scribano, C.M., Lynch, A.R., Carlsen, C.L., Pop-Vicas, S.T., Pattaswamy, S.M., Burkard, M.E., and Weaver, B.A. (2023). Diverse microtubule-targeted anticancer agents kill cells by inducing chromosome missegregation on multipolar spindles. *PLoS Biol.* 21, e3002339. <https://doi.org/10.1371/journal.pbio.3002339>.
 21. Zasadil, L.M., Andersen, K.A., Yeum, D., Rocque, G.B., Wilke, L.G., Tevaarwerk, A.J., Raines, R.T., Burkard, M.E., and Weaver, B.A. (2014). Cytotoxicity of paclitaxel in breast cancer is due to chromosome missegregation on multipolar spindles. *Sci. Transl. Med.* 6, 229ra43. <https://doi.org/10.1126/scitranslmed.3007965>.
 22. Bode, C.J., Gupta, M.L., Jr., Reiff, E.A., Suprenant, K.A., Georg, G.I., and Himes, R.H. (2002). Epothilone and paclitaxel: unexpected differences in promoting the assembly and stabilization of yeast microtubules. *Biochemistry* 41, 3870–3874. <https://doi.org/10.1021/bi0121611>.
 23. Geyer, E.A., Burns, A., Lalonde, B.A., Ye, X., Piedra, F.A., Huffaker, T.C., and Rice, L.M. (2015). A mutation uncouples the tubulin conformational and GTPase cycles, revealing allosteric control of microtubule dynamics. *Elife* 4, e10113. <https://doi.org/10.7554/elife.10113>.
 24. Machin, N.A., Lee, J.M., and Barnes, G. (1995). Microtubule stability in budding yeast: characterization and dosage suppression of a benomyl-dependent tubulin mutant. *Mol. Biol. Cell* 6, 1241–1259. <https://doi.org/10.1091/mbc.6.9.1241>.
 25. Kavallaris, M. (2010). Microtubules and resistance to tubulin-binding agents. *Nat. Rev. Cancer* 10, 194–204. <https://doi.org/10.1038/nrc2803>.
 26. Hickman, M.J., and Winston, F. (2007). Heme levels switch the function of Hap1 of *Saccharomyces cerevisiae* between transcriptional activator and transcriptional repressor. *Mol. Cell Biol.* 27, 7414–7424. <https://doi.org/10.1128/MCB.00887-07>.
 27. Biggins, S. (2013). The composition, functions, and regulation of the budding yeast kinetochore. *Genetics* 194, 817–846. <https://doi.org/10.1534/genetics.112.145276>.
 28. Fischbock-Halwachs, J., Singh, S., Potocnjak, M., Hagemann, G., Solis-Mezarino, V., Woike, S., Ghodgaonkar-Steger, M., Weissmann, F., Gallego, L.D., Rojas, J., et al. (2019). The COMA complex interacts with Cse4 and positions Sli15/lpl1 at the budding yeast inner kinetochore. *Elife* 8, e42879. <https://doi.org/10.7554/elife.42879>.
 29. Johnson, V., Ayaz, P., Huddleston, P., and Rice, L.M. (2011). Design, over-expression, and purification of polymerization-blocked yeast alphabeta-tubulin mutants. *Biochemistry* 50, 8636–8644. <https://doi.org/10.1021/bi2005174>.
 30. Humphrey, L., Felzer-Kim, I., and Joglekar, A.P. (2018). Stu2 acts as a microtubule destabilizer in metaphase budding yeast spindles. *Mol. Biol. Cell* 29, 247–255. <https://doi.org/10.1091/mbc.E17-08-0494>.
 31. van Breugel, M., Drechsel, D., and Hyman, A. (2003). Stu2p, the budding yeast member of the conserved Dis1/XMAP215 family of microtubule-associated proteins is a plus end-binding microtubule destabilizer. *J. Cell Biol.* 161, 359–369. <https://doi.org/10.1083/jcb.200211097>.
 32. Krenn, V., and Musacchio, A. (2015). The Aurora B Kinase in Chromosome Bi-Orientation and Spindle Checkpoint Signaling. *Front. Oncol.* 5, 225. <https://doi.org/10.3389/fonc.2015.00225>.
 33. Keyes, B.E., and Burke, D.J. (2009). Irc15 is a microtubule-associated protein that regulates microtubule dynamics in *Saccharomyces cerevisiae*. *Curr. Biol.* 19, 472–478. <https://doi.org/10.1016/j.cub.2009.01.068>.
 34. Duffy, S., Fam, H.K., Wang, Y.K., Styles, E.B., Kim, J.H., Ang, J.S., Singh, T., Larionov, V., Shah, S.P., Andrews, B., et al. (2016). Overexpression screens identify conserved dosage chromosome instability genes in yeast and human cancer. *Proc. Natl. Acad. Sci. USA* 113, 9967–9976. <https://doi.org/10.1073/pnas.1611839113>.
 35. Kumar, A., Meier, S.M., Farcas, A.M., Manatschal, C., Barral, Y., and Steinmetz, M.O. (2021). Structure and regulation of the microtubule plus-end tracking protein Kar9. *Structure* 29, 1266–1278.e4. <https://doi.org/10.1016/j.str.2021.06.012>.
 36. Bergman, Z.J., Wong, J.J., Drubin, D.G., and Barnes, G. (2023). Cik1 and Vik1 accessory proteins confer distinct functions to the kinesin-14 Kar3. *J. Cell Sci.* 136, jcs260621. <https://doi.org/10.1242/jcs.260621>.
 37. Zhu, Y.O., Siegal, M.L., Hall, D.W., and Petrov, D.A. (2014). Precise estimates of mutation rate and spectrum in yeast. *Proc. Natl. Acad. Sci. USA* 111, E2310–E2318. <https://doi.org/10.1073/pnas.1323011111>.
 38. Pompei, S., and Cosentino Lagomarsino, M. (2023). A fitness trade-off explains the early fate of yeast aneuploids with chromosome gains. *Proc. Natl. Acad. Sci. USA* 120, e2211687120. <https://doi.org/10.1073/pnas.2211687120>.
 39. Adell, M.A.Y., Klockner, T.C., Höfler, R., Wallner, L., Schmid, J., Markovic, A., Martyniak, A., and Campbell, C.S. (2023). Adaptation to spindle assembly checkpoint inhibition through the selection of specific aneuploidies. *Genes Dev.* 37, 171–190. <https://doi.org/10.1101/gad.350182.122>.
 40. Miller, M.P., Asbury, C.L., and Biggins, S. (2016). A TOG Protein Confers Tension Sensitivity to Kinetochore-Microtubule Attachments. *Cell* 165, 1428–1439. <https://doi.org/10.1016/j.cell.2016.04.030>.
 41. Wolnyiak, M.J., Blake-Hodek, K., Kosco, K., Hwang, E., You, L., and Huffaker, T.C. (2006). The regulation of microtubule dynamics in *Saccharomyces cerevisiae* by three interacting plus-end tracking proteins. *Mol. Biol. Cell* 17, 2789–2798. <https://doi.org/10.1091/mbc.e05-09-0892>.
 42. Geyer, E.A., Miller, M.P., Brautigam, C.A., Biggins, S., and Rice, L.M. (2018). Design principles of a microtubule polymerase. *Elife* 7, e34574. <https://doi.org/10.7554/elife.34574>.
 43. Yu, J.X., Chen, Q., Yu, Y.Q., Li, S.Q., and Song, J.F. (2016). Upregulation of colonic and hepatic tumor overexpressed gene is significantly associated

- with the unfavorable prognosis marker of human hepatocellular carcinoma. *Am. J. Cancer Res.* 6, 690–700.
44. Charrasse, S., Mazel, M., Taviaux, S., Berta, P., Chow, T., and Larroque, C. (1995). Characterization of the cDNA and pattern of expression of a new gene over-expressed in human hepatomas and colonic tumors. *Eur. J. Biochem.* 234, 406–413. https://doi.org/10.1111/j.1432-1033.1995.406_b.x.
 45. De, S., Cipriano, R., Jackson, M.W., and Stark, G.R. (2009). Overexpression of kinesins mediates docetaxel resistance in breast cancer cells. *Cancer Res.* 69, 8035–8042. <https://doi.org/10.1158/0008-5472.CAN-09-1224>.
 46. He, L., Yang, C.P., and Horwitz, S.B. (2001). Mutations in beta-tubulin map to domains involved in regulation of microtubule stability in epothilone-resistant cell lines. *Mol. Cancer Therapeut.* 1, 3–10.
 47. Barlow, S.B., Gonzalez-Garay, M.L., and Cabral, F. (2002). Paclitaxel-dependent mutants have severely reduced microtubule assembly and reduced tubulin synthesis. *J. Cell Sci.* 115, 3469–3478. <https://doi.org/10.1242/jcs.115.17.3469>.
 48. Yin, S., Zeng, C., Hari, M., and Cabral, F. (2012). Random mutagenesis of beta-tubulin defines a set of dispersed mutations that confer paclitaxel resistance. *Pharm. Res. (N. Y.)* 29, 2994–3006. <https://doi.org/10.1007/s11095-012-0794-5>.
 49. Wang, W., Zhang, H., Wang, X., Patterson, J., Winter, P., Graham, K., Ghosh, S., Lee, J.C., Katsetos, C.D., Mackey, J.R., et al. (2017). Novel mutations involving betal-betaIIA- or betalVIB-tubulin isoforms with functional resemblance to betall-tubulin in breast cancer. *Protoplasma* 254, 1163–1173. <https://doi.org/10.1007/s00709-016-1060-1>.
 50. Longtine, M.S., McKenzie, A., 3rd, Demarini, D.J., Shah, N.G., Wach, A., Brachat, A., Philippson, P., and Pringle, J.R. (1998). Additional modules for versatile and economical PCR-based gene deletion and modification in *Saccharomyces cerevisiae*. *Yeast* 14, 953–961. [https://doi.org/10.1002/\(SICI\)1097-0061\(199807\)14:10<953::AID-YEA293>3.0.CO;2-U](https://doi.org/10.1002/(SICI)1097-0061(199807)14:10<953::AID-YEA293>3.0.CO;2-U).
 51. Huber, F., Meurer, M., Bunina, D., Kats, I., Maeder, C.I., Stefl, M., Mongis, C., and Knop, M. (2014). PCR Duplication: A One-Step Cloning-Free Method to Generate Duplicated Chromosomal Loci and Interference-Free Expression Reporters in Yeast. *PLoS One* 9, e114590. <https://doi.org/10.1371/journal.pone.0114590>.
 52. Pavelka, N., Rancati, G., Zhu, J., Bradford, W.D., Saraf, A., Florens, L., Sanderson, B.W., Hattem, G.L., and Li, R. (2010). Aneuploidy confers quantitative proteome changes and phenotypic variation in budding yeast. *Nature* 468, 321–325. <https://doi.org/10.1038/nature09529>.
 53. Zhu, J., Pavelka, N., Bradford, W.D., Rancati, G., and Li, R. (2012). Karyotypic determinants of chromosome instability in aneuploid budding yeast. *PLoS Genet.* 8, e1002719. <https://doi.org/10.1371/journal.pgen.1002719>.
 54. Weaver, S., Dube, S., Mir, A., Qin, J., Sun, G., Ramakrishnan, R., Jones, R.C., and Livak, K.J. (2010). Taking qPCR to a higher level: Analysis of CNV reveals the power of high throughput qPCR to enhance quantitative resolution. *Methods* 50, 271–276. <https://doi.org/10.1016/j.ymeth.2010.01.003>.
 55. Bolger, A.M., Lohse, M., and Usadel, B. (2014). Trimmomatic: a flexible trimmer for Illumina sequence data. *Bioinformatics* 30, 2114–2120. <https://doi.org/10.1093/bioinformatics/btu170>.
 56. Li, H., and Durbin, R. (2010). Fast and accurate long-read alignment with Burrows-Wheeler transform. *Bioinformatics* 26, 589–595. <https://doi.org/10.1093/bioinformatics/btp698>.
 57. Faust, G.G., and Hall, I.M. (2014). SAMBLASTER: fast duplicate marking and structural variant read extraction. *Bioinformatics* 30, 2503–2505. <https://doi.org/10.1093/bioinformatics/btu314>.
 58. Li, H., Handsaker, B., Wysoker, A., Fennell, T., Ruan, J., Homer, N., Marth, G., Abecasis, G., and Durbin, R.; 1000 Genome Project Data Processing Subgroup (2009). The Sequence Alignment/Map format and SAMtools. *Bioinformatics* 25, 2078–2079. <https://doi.org/10.1093/bioinformatics/btp352>.
 59. McKenna, A., Hanna, M., Banks, E., Sivachenko, A., Cibulskis, K., Kerntsky, A., Garimella, K., Altshuler, D., Gabriel, S., Daly, M., and DePristo, M.A. (2010). The Genome Analysis Toolkit: a MapReduce framework for analyzing next-generation DNA sequencing data. *Genome Res.* 20, 1297–1303. <https://doi.org/10.1101/gr.107524.110>.
 60. Pipek, O., Ribli, D., Molnár, J., Póti, Á., Krzystanek, M., Bodor, A., Tusnády, G.E., Szallasi, Z., Csabai, I., and Szűts, D. (2017). Fast and accurate mutation detection in whole genome sequences of multiple isogenic samples with IsoMut. *BMC Bioinf.* 18, 73. <https://doi.org/10.1186/s12859-017-1492-4>.
 61. Kimura, M. (1962). On the probability of fixation of mutant genes in a population. *Genetics* 47, 713–719. <https://doi.org/10.1093/genetics/47.6.713>.
 62. Lassig, M. (2007). From biophysics to evolutionary genetics: statistical aspects of gene regulation. *BMC Bioinf.* 8, S7. <https://doi.org/10.1186/1471-2105-8-S6-S7>.
 63. Luria, S.E., and Delbrück, M. (1943). Mutations of Bacteria from Virus Sensitivity to Virus Resistance. *Genetics* 28, 491–511. <https://doi.org/10.1093/genetics/28.6.491>.

STAR★METHODS

KEY RESOURCES TABLE

REAGENT or RESOURCE	SOURCE	IDENTIFIER
Antibodies		
Anti Tub1	Bio-Rad	Cat# MCA78G; RRID:AB_325005
FITC-conjugated Anti Rat	Jackson ImmunoResearch Laboratories	712-095-153
Chemicals, peptides, and recombinant proteins		
Dimethyl sulfoxide, DMSO	SigmaAldrich	276855-250ML
Benomyl powder	SigmaAldrich	45339-250MG
alpha-factor powder	GenScript	RP01002
G-418	Thermofisher	11811-031
Penicillin-Streptomycin 100X	Bio West	L0022
Propidium iodide	SigmaAldrich	25535-16-6
RNAse (Ribonuclease A from bovine pancreas)	SigmaAldrich	R5503
Critical commercial assays		
SYBR Green master mix	Roche	04887352001
Maxwell® RSC simplyRNA Tissue Kit	Promega	AS1340
SuperScript VIVO cDNA Synthesis Kit	Thermofisher	11754050
Deposited data		
NGS data	Database: EBI-EMBL Array	E-MTAB-14739
Experimental models: Organisms/strains		
yAC488	Our Lab	MAT α , mad2 Δ ::His3MX
yAC4553	Our Lab	MATA/ α , ura3::URA3 (1x)/ura3::URA3(1x), trp1::TRP1 (2x)/trp1::TRP1 (2x), TUB2/TUB2::KanMX
yAC4554	Our Lab	MATA/ α , ura3::URA3 (1x)/ura3::URA3(1x), trp1::TRP1 (2x)/trp1::TRP1 (2x), TUB2/tub2 ^{T238A} ::KanMX
yAC4772	Our Lab	MATA/ α , ura3::URA3 (1x)/ura3::URA3(1x), trp1::TRP1 (2x)/trp1::TRP1 (2x), TUB2/tub2 ^{Y422C} ::KanMX
yAC4837	Our Lab	MATA/ α , ura3::URA3 (1x)/ura3::URA3(1x), trp1::TRP1 (2x)/trp1::TRP1 (2x), TUB2/tub2 ^{T238A,Y422C} ::KanMX
yAC4838	Our Lab	MATA, ura3::URA3 (1x), trp1::TRP1 (2x), tub2 ^{Y422C} ::KanMX
yAC4839	Our Lab	MATA, ura3::URA3 (1x), trp1::TRP1 (2x), tub2 ^{T238A,Y422C} ::KanMX
yAC4921	Our Lab	MATA/ α , ura3::URA3 (1x)/ura3::URA3(1x), trp1::TRP1 (2x)/trp1::TRP1 (2x), TUB2/tub2 ^{T238A} ::KanMX, STU2/STU2-2X::LEU2
yAC4922	Our Lab	MATA/ α , ura3::URA3 (1x)/ura3::URA3(1x), trp1::TRP1 (2x)/trp1::TRP1 (2x), TUB2/tub2 ^{T238A} ::KanMX, IPL1/IPL1-2X::LEU2
yAC4926	Our Lab	MATA, ura3::URA3 (1x), trp1::TRP1 (2x), TUB2::KanMX, STU2-2X::LEU2
yAC4930	Our Lab	MATA/ α , ura3::URA3 (1x)/ura3::URA3(1x), trp1::TRP1 (2x)/trp1::TRP1 (2x), TUB2/tub2 ^{T238A,H396N} ::KanMX
yAC4931	Our Lab	MATA, ura3::URA3 (1x), trp1::TRP1 (2x), tub2 ^{T238A,H396N} ::KanMX

(Continued on next page)

Continued

REAGENT or RESOURCE	SOURCE	IDENTIFIER
yAC4932	Our Lab	MATa/α, <i>ura3</i> ::URA3 (1x)/ <i>ura3</i> ::URA3(1x), <i>trp1</i> ::TRP1 (2x)/ <i>trp1</i> ::TRP1 (2x), TUB2/TUB2::KanMX, TUB1/tub1 ^{V289L} ::His3MX
yAC4933	Our Lab	MATa/α, <i>ura3</i> ::URA3 (1x)/ <i>ura3</i> ::URA3(1x), <i>trp1</i> ::TRP1 (2x)/ <i>trp1</i> ::TRP1 (2x), TUB2/tub2 ^{T238A} ::KanMX, TUB1/tub1 ^{V289L} ::His3MX
yAC4934	Our Lab	MATa, <i>ura3</i> ::URA3 (1x), <i>trp1</i> ::TRP1 (2x), TUB2::KanMX, tub1 ^{V289L} ::His3MX
yAC4935	Our Lab	MATa, <i>ura3</i> ::URA3 (1x), <i>trp1</i> ::TRP1 (2x), tub2 ^{T238A} ::KanMX, tub1 ^{V289L} ::His3MX
yAC4946	Our Lab	MATa/α, <i>ura3</i> ::URA3 (1x)/ <i>ura3</i> ::URA3(1x), <i>trp1</i> ::TRP1 (2x)/ <i>trp1</i> ::TRP1 (2x), TUB2/tub2 ^{N347K} ::KanMX
yAC4948	Our Lab	MATa/α, <i>ura3</i> ::URA3 (1x)/ <i>ura3</i> ::URA3(1x), <i>trp1</i> ::TRP1 (2x)/ <i>trp1</i> ::TRP1 (2x), TUB2/tub2 ^{T238A,Q291P} ::KanMX
yAC4949	Our Lab	MATa/α, <i>ura3</i> ::URA3 (1x)/ <i>ura3</i> ::URA3(1x), <i>trp1</i> ::TRP1 (2x)/ <i>trp1</i> ::TRP1 (2x), TUB2/tub2 ^{V326M} ::KanMX
yAC4951	Our Lab	MATa, <i>ura3</i> ::URA3 (1x), <i>trp1</i> ::TRP1 (2x), tub2 ^{N347K} ::KanMX
yAC4953	Our Lab	MATa, <i>ura3</i> ::URA3 (1x), <i>trp1</i> ::TRP1 (2x), tub2 ^{T238A,Q291P} ::KanMX
yAC4960	Our Lab	MATa/α, <i>ura3</i> ::URA3 (1x)/ <i>ura3</i> ::URA3(1x), <i>trp1</i> ::TRP1 (2x)/ <i>trp1</i> ::TRP1 (2x), TUB2/tub2 ^{T238A,V326M} ::KanMX
yAC4961	Our Lab	MATa/α, <i>ura3</i> ::URA3 (1x)/ <i>ura3</i> ::URA3(1x), <i>trp1</i> ::TRP1 (2x)/ <i>trp1</i> ::TRP1 (2x), TUB2/tub2 ^{H396N} ::KanMX
yAC4962	Our Lab	MATa, <i>ura3</i> ::URA3 (1x), <i>trp1</i> ::TRP1 (2x), tub2 ^{T238A,V326M} ::KanMX
yAC4965	Our Lab	MATa/α, <i>ura3</i> ::URA3 (1x)/ <i>ura3</i> ::URA3(1x), <i>trp1</i> ::TRP1 (2x)/ <i>trp1</i> ::TRP1 (2x), TUB2/tub2 ^{T238A} ::KanMX, IPL1/IPL1-2X::LEU2, CTF19/CTF19-2X::His3MX,
yAC4977	Our Lab	MATa/α, <i>ura3</i> ::URA3 (1x)/ <i>ura3</i> ::URA3(1x), <i>trp1</i> ::TRP1 (2x)/ <i>trp1</i> ::TRP1 (2x), TUB2/tub2 ^{Q291P} ::KanMX
yAC4978	Our Lab	MATa/α, <i>ura3</i> ::URA3 (1x)/ <i>ura3</i> ::URA3(1x), <i>trp1</i> ::TRP1 (2x)/ <i>trp1</i> ::TRP1 (2x), TUB2/tub2 ^{V268I} ::KanMX
yAC4979	Our Lab	MATa/α, <i>ura3</i> ::URA3 (1x)/ <i>ura3</i> ::URA3(1x), <i>trp1</i> ::TRP1 (2x)/ <i>trp1</i> ::TRP1 (2x), TUB2/tub2 ^{T238A,V268I} ::KanMX
yAC4980	Our Lab	MATa, <i>ura3</i> ::URA3 (1x), <i>trp1</i> ::TRP1 (2x), tub2 ^{V268I} ::KanMX
yAC4981	Our Lab	MATa, <i>ura3</i> ::URA3 (1x), <i>trp1</i> ::TRP1 (2x), tub2 ^{T238A,V268I} ::KanMX
yAC4982	Our Lab	MATa/α, <i>ura3</i> ::URA3 (1x)/ <i>ura3</i> ::URA3(1x), <i>trp1</i> ::TRP1 (2x)/ <i>trp1</i> ::TRP1 (2x), TUB2/tub2 ^{T238A} ::KanMX, IPL1/IPL1-2X::LEU2, CTF19/CTF19-2X::His3MX, MCM16/MCM16-2X::hphNT1
yAC4983	Our Lab	MATa/α, <i>ura3</i> ::URA3 (1x)/ <i>ura3</i> ::URA3(1x), <i>trp1</i> ::TRP1 (2x)/ <i>trp1</i> ::TRP1 (2x), TUB2/tub2 ^{T238S} ::KanMX
yAC4985	Our Lab	MATa, <i>ura3</i> ::URA3 (1x), <i>trp1</i> ::TRP1 (2x), tub2 ^{T238S} ::KanMX
yAC4998	Our Lab	MATa, <i>ura3</i> ::URA3 (1x), <i>trp1</i> ::TRP1 (2x), TUB2::KanMX
yAC4999	Our Lab	MATa/α, <i>ura3</i> ::URA3 (1x)/ <i>ura3</i> ::URA3(1x), <i>trp1</i> ::TRP1 (2x)/ <i>trp1</i> ::TRP1 (2x), TUB2/tub2 ^{T238A,N347K} ::KanMX

(Continued on next page)

Continued

REAGENT or RESOURCE	SOURCE	IDENTIFIER
yAC5000	Our Lab	MATA, ura3::URA3 (1x), trp1::TRP1 (2x), tub2 ^{T238A,N347K} ::KanMX
yAC5003	Our Lab	MATA, ura3::URA3 (1x), trp1::TRP1 (2x), tub2 ^{T238S} ::KanMX, STU2-2X::LEU2
yAC5089	Our Lab	MATA, his3-11,15::HIS3tetR-GFP (single integration), ura3::3XURA3tetO112
yAC5091	Our Lab	MATA, his3-11,15::HIS3tetR-GFP (single integration), ura3::3XURA3tetO112, tub2 ^{T238S} ::KanM
yAC5092	Our Lab	MATA, his3-11,15::HIS3tetR-GFP (single integration), ura3::3XURA3tetO112, tub2 ^{T238S} ::KanMX, STU2-2X::LEU2
yAC5112	Our Lab	MATA/α, ura3::URA3 (1x)/ura3::URA3(1x), trp1::TRP1 (2x)/trp1::TRP1 (2x), TUB2/tub2 ^{T238A} ::KanMX, IPL1/ipl1 Δ::His3MX, leu2/leu2::IPL1::LEU2
yAC5261	Our Lab	MATA/α, ura3::URA3 (1x)/ura3::URA3(1x), trp1::TRP1 (2x)/trp1::TRP1 (2x), TUB2/tub2 ^{T238A} ::KanMX, MCM21/mcm21 ^{E159D} ::His3MX
yAC5321	Our Lab	MATA/α, ura3::URA3 (1x)/ura3::URA3(1x), trp1::TRP1 (2x)/trp1::TRP1 (2x), TUB2/tub2 ^{T238A} ::KanMX, IRC15/IRC15-2X::LEU2
yAC5322	Our Lab	MATA/α, ura3::URA3 (1x)/ura3::URA3(1x), trp1::TRP1 (2x)/trp1::TRP1 (2x), TUB2/tub2 ^{T238A} ::KanMX, KAR9/KAR9-2X::LEU2
yAC5456	Our Lab	MATA/α, ura3::URA3 (1x)/ura3::URA3(1x), trp1::TRP1 (2x)/trp1::TRP1 (2x), TUB2/tub2 ^{T238A,A302P} ::KanMX
yAC5462	Our Lab	MATA/α, ura3::URA3 (1x)/ura3::URA3(1x), trp1::TRP1 (2x)/trp1::TRP1 (2x), TUB2/tub2 ^{A302P} ::KanMX

Oligonucleotides

Mad2 deletion_Reverse	SigmaAldrich	AAAACGAGATTTTTGGACTTCCGTCTTTTTTTTT TTGACTTGAATTCTATTAAATCGATGAATTCGAGCTCG
Mad2 deletion_Forward	SigmaAldrich	GTCACAGAGTATTGAAAACCACTCAAAGGGGCC AATAGCACATTAAATGCGTACGCTGCAGGTCGAC
TUB2 mutagenesis to T238A_Reverse	SigmaAldrich	TCATGTCTGGTGTGACAGCCTCATGCGTTATCCG
TUB2 mutagenesis to T238A_Reverse	SigmaAldrich	CGGGATAACGCAATGAAGCTGTCACACCAGACATGA
RIM1_qPCR_Forward	SigmaAldrich	GTTAGAAAAGGGTATGTTATTGGTATATG
RIM1_qPCR_Reverse	SigmaAldrich	AACCGTCGTCTCTCGAAG
TUB1 cloning_Forward	SigmaAldrich	CGCGGATCCATGAGAGAAGTTATTAGTATTAATG
TUB1 cloning_Reverse	SigmaAldrich	CCTTAATTAAAGGGTGAAAAACCTGATAATATCG
TUB1 gene replacement_Forward	SigmaAldrich	CCACCCAAGATCTGAAACTTACAAC TGCAAACAAACAA TGAGAGAAGTTATTAGTATGGTATGTCGATTGCC
TUB1 gene replacement_Reverse	SigmaAldrich	GAAAGGATAAGGAGGTTGGGGCGAGAGTGAACC ATCGATGAATCGAGCTCGTTAACTGGATGGC
TUB2 cloning_Forward	SigmaAldrich	CACCCGGGATGAGAGAAATCATTCTATCTCG
TUB2 cloning_Reverse	SigmaAldrich	CCCTTAATTAAATTAGTCTCAACAAATTCTGGGG
TUB2 gene replacement_Forward	SigmaAldrich	CTACAACTACAAAAGCAAATCTCCACAAAGTAATAT AATGAGAGAAATCATTCTCGACAGGTCAGTG
TUB2 gene replacement_Reverse	SigmaAldrich	ATGGAAATCACAAATAAAACACAGTTTTGTTCAT GATCGATGAATCGAGCTCGTTAACTGGATGGC
TUB1 mutagenesis to V289L_Forward	SigmaAldrich	CATTCCATGAGTCCAAC TCTCTGT CAGAAATTACAAACCGCTT

(Continued on next page)

Continued

REAGENT or RESOURCE	SOURCE	IDENTIFIER
TUB1 mutagenesis to V289L_Reverse	SigmaAldrich	CAAGCGTTGTAATTCTGACAGA GAGTTGGACTCATGGAATG
TUB2 mutagenesis to Y422C_Forward	SigmaAldrich	TGATCTGGTAGCGAACATGCCAACATA CCAGAGG
TUB2 mutagenesis to Y422C_Reverse	SigmaAldrich	GCCTCTGGTATTGGCATTGCTAAC CAGATCA
IPL1_duplication_Forward	SigmaAldrich	ATCAAAAGGCTTACATTATTA AAAAAATTCAAACATA TAGATGACAAGTACGGCAACTGTGGAA ACTCTAG
IPL1_duplication_Reverse	SigmaAldrich	AAGTGAATCCACTAAGAATATCA ACGGATGGCTGAAGTT TTCTCGAAAAATAGAACATATTCCATT TTGTAATTCTGTG
STU2_duplication_Forward	SigmaAldrich	ATTTAAAAGATTATGCTTCTGACT TTTCGTTGAA ATGAGGCTCGTGGAA ACCACTGTGGAA ACTCTAG
STU2_duplication_Reverse	SigmaAldrich	ATTAGAAATTGACTACTCTGACA ATGGTTCTACC CAGCAATATCCCAGGAACATATTCCATT TTGTAATTCTGTG
TUB2 mutagenesis to N347K_Forward	SigmaAldrich	ATTCGTGGAATGGAT CCCCAAAAA TGTGCAA ACTGCTGTGT
TUB2 mutagenesis to N347K_Reverse	SigmaAldrich	ACACACAGCAGTTG CACATT GGGGATCCATT CACGAA
TUB2 mutagenesis to Q219P_Forward	SigmaAldrich	TCTTGACTG TCCCTG TAACAC CGCAA ATGTTGAT GCCAAGAACAT
TUB2 mutagenesis to Q219P_Reverse	SigmaAldrich	ATGTTCTGG CATCAA ACATTG GGCG TGTTAAC CAGGGACAG CTAAAGA
TUB2 mutagenesis to V326M_Forward	SigmaAldrich	AGAGGTAAAG TTCCGTTA AGGAGA TGGAA GATG CAATAAGTGC
TUB2 mutagenesis to V326M_Reverse	SigmaAldrich	GCAC TTATGC ATTTCAT CTTCCA TCTC CTTAAC GGAA ACTTAC CTCT
TUB2 mutagenesis to V268I_Forward	SigmaAldrich	CCAC GTTTAC ATTTCT CATG TCGG CTACG CTCCATT GACG
TUB2 mutagenesis to V268I_Reverse	SigmaAldrich	CGTCA ATGGAG CGTAG CCGAT CA TGAAG AAATGT AAACGT GG
TUB2 mutagenesis to H396N_Forward	SigmaAldrich	GCTATGTT CAAAGAAA AGCTTTCTG AACTGGT ATACTAGT GAAGGT ATGGA
TUB2 mutagenesis to H396N_Reverse	SigmaAldrich	TCC ATAC CTTCA CTAGT TACCA GTT CAAG AAAGC TTTCT TTGA ACATAGC
CTF19_duplication_Forward	SigmaAldrich	ACCA ATGCT GGAA ATATCT AAAC CTTTAG CAGGG GAC GTCT ACCA ATAGAA ACC ACT CACT TAC AGGG GAG ACCG
CTF19_duplication_Reverse	SigmaAldrich	ATTTGG CTATTAG AGCG AACAG CAGA GAGA ATT TGT CCTT GG TTTC CAGAG TTG GAA AGG AT CCCC GGGT TA ATT AAGG
TUB2 mutagenesis to T238S_Forward	SigmaAldrich	TCAT GTCT GGGT GTGAC ATCT CATT GCGT TAT CCCG
TUB2 mutagenesis to T238S_Reverse	SigmaAldrich	CGGG GATA ACG CAAT GAAG ATGT CAC ACCC AGAC ATGA
TUB2 mutagenesis to A302P_Forward	SigmaAldrich	CCAAG AACAT GAT GGCT CCT GCCG ATCCA AGAAA
TUB2 mutagenesis to A302P_Reverse	SigmaAldrich	TTT CTTGG ATCGGC AGGG GCCAT CAT GTTCT GG
MCM16_duplication_Forward	SigmaAldrich	ACAGA AGAG ATGAA TTG ACAAA ACT CACT ATCC GGTA TTCC ACCA ATG GAAG GGTT TAG CTTGC CTCG CCCC
MCM16_duplication_Reverse	SigmaAldrich	GTT GAA ATGG GTGG CAGT GTGA ATT AGAG GAGA AGAAA GAGA AGGG CAG AAAG ATT GGAT GGCG CGTT AGT ATC
IPL1_qPCR_Forward	SigmaAldrich	AACGG ACT TCGG ATGG GAGTA
IPL1_qPCR_Reverse	SigmaAldrich	CCGG TCAGT AGTT CAA ACGC
STU2_qPCR_Forward	SigmaAldrich	AACGT CCT CAAGGG CTACAA

(Continued on next page)

Continued

REAGENT or RESOURCE	SOURCE	IDENTIFIER
STU2_qPCR_Reverse	SigmaAldrich	CGAATGCAGCCATCACTCA
IPL1_deletion_Forward	SigmaAldrich	AAACTGGGATTGAAATACAACAAAAGAAAGAAGTAA AAGGGATGCAACGCAATACGTACGCTGCAGGTCGAC
IPL1_deletion_Reverse	SigmaAldrich	ATATGTGCAGGAGTGATTAATGTGCCCTCAAACGAT TCTGTCTACTTTAATTCTAACTGATGAATTGAGCTCG
IPL1_cloning_Forward	SigmaAldrich	CGCGGATCCTAGTATCATTATCCCTATCAAATT
IPL1_cloning_Reverse	SigmaAldrich	CCGAGCTCCGTAAGTGTCTATATGTTGAA
LEU_replacement_Forward	SigmaAldrich	TTAACAGAAGGATTCTTAACCTCTCGGCGACAG CATTAGTATCATTATCCCTATCAAATTATTTTGCG
LEU_replacement_Reverse	SigmaAldrich	ACTGTGGGAATACTCAGGTATCGTAAGATGCAAGA GTTGAATCTCTTAGCAACCATTATTTTCTC
MCM21_cloning_Forward	SigmaAldrich	CGCGGATCCATGAGTAGAACATGATGATTA
MCM21_cloning_Reverse	SigmaAldrich	CCTTAATTAAATTGGCCTCTGCTAAAAATAG
MCM21 mutagenesis to E159DForward	SigmaAldrich	AGTACAAGTGTAGAAGTGAAGTGCAGT GAAGATTATATTGCTCTGG
MCM21 mutagenesis to E159D_Reverse	SigmaAldrich	CCAGGACAATAATCTTCCAAGT CACTTCTATCACCTGTACT
MCM21 replacement_Forward	SigmaAldrich	CTTCAAACATACAGTAACGCTCTGGCAATGAG TAGAATCGATGATTACAGCAGGACATTGAATCTT
MCM21 replacement_Reverse	SigmaAldrich	ATCCTCTTCTATAAAAGTATAATTGTTAACATC ATCGATGAATTGAGCTCGTTAAACTGGATGGC
KAR9_duplication_Forward	SigmaAldrich	GCGCGAACATGGAAGTACTGTGAGAAGAAGCATAAG GTCGATTTAGAAGAGCCAACTGTGGGAATACTCG
KAR9_duplication_Reverse	SigmaAldrich	GGTCAGATGGCCCAGGAGCCGCTTCTCATTAAGTATTG CGATAAAGCACTGTGAACATATCCATTGTAATTCTGT
IRC15_duplication_Forward	SigmaAldrich	TTTCAGAAATTATAATTGACCACAAACTTCAT CCCATCGTTATGTAACCTCCAACTGTGGGAATACTCAG
IRC15_duplication_Reverse	SigmaAldrich	AACAATTTATACCGCAAACACTATACGGCAAGGCAAC TGATTACACTTGTGAACATATCCATTGTAATTCTGT
IRC15_qPCR_Forward	SigmaAldrich	CGATGTCCTGGTAATTGGTT
IRC15_qPCR_Reverse	SigmaAldrich	TGCTCGATAAGTCTTGCTG
CTF19_qPCR_Forward	SigmaAldrich	CGCATTAAAGTCTGGAAGACG
CTF19_qPCR_Reverse	SigmaAldrich	TGGTACGTGGATCTTGT
MCM16_qPCR_Reverse	SigmaAldrich	AGGAGCACGTGGAGGTATATA
MCM16_qPCR_Reverse	SigmaAldrich	TTGGTATTGTCGGTTCTCC
KAR9_qPCR_Forward	SigmaAldrich	AAGACTCAGTTGGAGCCATG
KAR9_qPCR_Reverse	SigmaAldrich	TGATGGAGTATGCCGTATCGG
KAR3_qPCR_Forward	SigmaAldrich	GCTATGAATGCCACAAAGAAG
KAR3_qPCR_Reverse	SigmaAldrich	GAGTTGCTTCTGGTTCCAT
VIK1_qPCR_Forward	SigmaAldrich	CACGACAAACACCATGAATGG
VIK1_qPCR_Reverse	SigmaAldrich	CGCACTCAATCAATTGAGTCC
ChrVII_qPCR_Forward	SigmaAldrich	TGTGCGTCTCCCTAAAGCAGCTA
ChrVII_qPCR_Reverse	SigmaAldrich	GCATTGGATGCGATGAGATGGCAA
ChrXII_qPCR_Forward	SigmaAldrich	ATGGCAGGCAGGTGAATGAGATGA
ChrXII_qPCR_Reverse	SigmaAldrich	AGAGTAGACCATGGGACGTCGTT

Software and algorithms

FlowJo	Becton, Dickinson and Company	https://www.flowjo.com
Fiji	NIH	https://imagej.net/software/fiji/
R (version 4.0.3)	R-project	https://www.r-project.org/
MATLAB R2022A	MathWorks	https://it.mathworks.com/

(Continued on next page)

Continued

REAGENT or RESOURCE	SOURCE	IDENTIFIER
Isomut	Pipek O. BMC bioinformatics: Fast and accurate mutation detection in whole genome sequences of multiple isogenic samples with IsoMut	https://github.com/riblidezso/isomut
Other		
pAC 67	Gift from Foiani Lab	<i>pFA6a- KanMX6</i> [Longtine, 1998]
pAC 69	Gift from Foiani Lab	<i>pFA6A-His3MX6</i> [Longtine, 1998]
pAC161	Gift from Wei-Lih Lee Lab	<i>pHIS3p:mRuby2-Tub1+3'UTR::PH</i> [Markus SM, 2015]
pAC165	Gift from Branzei Lab	<i>Yiplac128-LEU2</i> [Gietz RD, 1988]
pAC184	Our Lab (this work)	<i>pFA6a- TUB2::KanMX6</i>
pAC185	Our Lab (this work)	<i>pFA6a- tub2^{T238A}::KanMX6</i>
pAC193	Our Lab (this work)	<i>pFA6a- tub2^{Y422C}::KanMX6</i>
pAC194	Our Lab (this work)	<i>pFA6a- tub2^{T238A, Y422C}::KanMX6</i>
pAC199	Our Lab (this work)	<i>pFA6A-TUB1::His3MX6</i>
pAC200	Our Lab (this work)	<i>pFA6a- tub2^{N347K}::KanMX6</i>
pAC201	Our Lab (this work)	<i>pFA6a- tub2^{T238A, N347K}::KanMX6</i>
pAC202	Our Lab (this work)	<i>pFA6a- tub2^{T238A, Q291P}::KanMX6</i>
pAC203	Our Lab (this work)	<i>pFA6a- tub2^{V326M}::KanMX6</i>
pAC204	Our Lab (this work)	<i>pFA6a- tub2^{T238A, V326M}::KanMX6</i>
pAC205	Our Lab (this work)	<i>pFA6a- tub2^{H396N}::KanMX6</i>
pAC205	Our Lab (this work)	<i>pFA6a- tub2^{T238A, H396N}::KanMX6</i>
pAC207	Our Lab (this work)	<i>pFA6A-tub1^{V289L}::His3MX6</i>
pAC208	Our Lab (this work)	<i>pFA6a- tub2^{Q291P}::KanMX6</i>
pAC209	Our Lab (this work)	<i>pFA6a- tub2^{V268I}::KanMX6</i>
pAC210	Our Lab (this work)	<i>pFA6a- tub2^{T238A, V268I}::KanMX6</i>
pAC211	Our Lab (this work)	<i>pFA6a- tub2^{T238S}::KanMX6</i>
pAC222	Our Lab (this work)	<i>Yiplac128-IPL1::LEU2</i>
pAC230	Our Lab (this work)	<i>pFA6A-MCM21::His3MX6</i>
pAC231	Our Lab (this work)	<i>pFA6A- mcm21^{E159D}::His3MX6</i>
pAC261	Our Lab (this work)	<i>pFA6a- tub2^{T238A, A302P}::KanMX6</i>

EXPERIMENTAL MODEL AND STUDY PARTICIPANT DETAILS

All yeast strains used are derivatives of or were 5 times backcrossed with W303 background. For the evolution experiment and the characterization of the compensatory genetic alterations we used a modified W303, prototroph for uracil and tryptophan (*ura3::URA3(1X) trp1:: TRP1 (2X)*). WT and *tub2^{T238A}* are isogenic, and both carry mutations in *BRO1*, *COS10*, *GPR1*, *MKT1*, *PDR10* and *VPS15*. To obtain *TUB2::KanMX*, *tub2^{T238A}::KanMX* and *tub2^{T238S}::KanMX* strains, the *TUB2* ORF and 494 bp downstream of the STOP codon were amplified from a WT strain (primers 523/524) and cloned into the XmaI/PacI sites of plasmid 67 (*pFA6a- KanMX6*) obtaining plasmid 184. *TUB2* gene on plasmid 184 was then mutagenized by site-directed mutagenesis (primers 397/398 and 783/784) to obtain plasmids 185 and 211, respectively. One copy of endogenous *TUB2* in a WT diploid strain was then replaced with *TUB2::KanMX*, *tub2^{T238A}::KanMX* and *tub2^{T238S}::KanMX* cassettes by one-step gene replacement.⁵⁰ The haploid strains *TUB2::KanMX*, *tub2^{T238A}::KanMX* and *tub2^{T238S}::KanMX* were obtained from the sporulation and the tetrad dissection of the diploids and selection on agar plates supplemented with Geneticin G-418 Sulfate (Thermo Fisher).

To obtain the compensatory mutants in tubulin, either alone or in combination with *tub2^{T238A}*, *TUB2* and *tub2^{T238A}* genes on plasmids 184 and 185 were mutagenized by site-directed mutagenesis and the *tub2::KanMX* cassettes carrying each mutagenized *TUB2* were used to replace one copy of the endogenous *TUB2* in a WT diploid strain by one-step gene replacement. The resulting haploid mutants were obtained from the sporulation and the tetrad dissection of the diploids and selection on G-418 plates.

To obtain the *tub1^{V289L}* mutant, *TUB1* ORF and 569 bp downstream of the STOP codon were amplified by PCR on a WT strain (primers 506/507) and cloned into the BamHI/PacI sites of plasmid 69 (*pFA6A-His3MX6*) obtaining plasmid 199. *TUB1::His3MX* on plasmid 199 was then mutagenized by site-directed mutagenesis (primers 620/621), to get plasmid 207. One copy of endogenous *TUB1* in *TUB2/tub2^{T238A}::KanMX* and *TUB2/TUB2::KanMX* diploids was then replaced with *tub1^{V289L}::His3MX* cassette by one-step

gene replacement. The haploid mutants $tub1^{V289L}::His3MX$ and $tub2^{T238A} tub1^{V289L}::His3MX$ were obtained from the sporulation and the tetrad dissection of the diploids and selection on G-418 and minus histidine plates.

To obtain the $mcm21^{E159D}$ mutant, *MCM21* ORF and 582 bp downstream of the STOP codon were amplified by PCR on a WT strain (primers 849/850) and cloned into the BamHI/PacI sites of the plasmid 69 (*pFA6A-His3MX6*). *MCM21::His3MX* on the resulting plasmid 230 was then mutagenized by site-directed mutagenesis (primers 851/852) obtaining plasmid 231. $mcm21^{E159D}::His3MX$ cassette was then used to replace one copy of the endogenous *MCM21* in a *TUB2/tub2^{T238A}::KanMX* diploid by one step gene replacement. The haploid mutants $mcm21^{E159D}::His3MX$ and $tub2^{T238A} mcm21^{E159D}::His3MX$ were obtained by sporulation of the diploids and selection on G-418 and minus histidine plates.

MAD2 and *IPL1* deletions were obtained by one step gene replacement of the endogenous copies with *His3MX* cassettes amplified from plasmid 69 (*pFA6A-His3MX6*) (primers 218/360 and 818/819, respectively).

To clone *IPL1* on chromosome III, *IPL1* ORF, 525 bp upstream of the ATG and 500 bp downstream of the STOP codon, were amplified by PCR on a WT strain (primers 822/824) and cloned into the BamHI/SacI sites of the plasmid 165 (*Yiplac128-LEU2*). *IPL1::LEU2* cassette was then amplified from the resulting plasmid 222 (primers 843/844) and used to replace endogenous *leu2* gene by one step gene replacement.

STU2, *IPL1*, *CTF19*, *MCM16*, *IRC15* and *KAR9* duplications, were performed according to.⁵¹ For *STU2*, *IPL1*, *IRC15* and *KAR9* duplications, *LEU2* from plasmid 165 (*Yiplac128-LEU2*) was amplified with primers 669/670, 667/668, 861/862 and 859/860, respectively. For *CTF19*, *His3MX* from plasmid 69 (*pFA6A-His3MX6*) was amplified with primers 771/772. For *MCM16* duplication, *hphNT1* from plasmid 161 (*pFA6A-hphNT1*) was amplified with primers 785/786.

Media and growth conditions

Cells were grown in YP medium (1% yeast extract, 2% Bacto Peptone, 50 mg/L adenine) supplemented with 2% glucose (YPD). For the evolution experiment, in liquid growth assays and immunofluorescence sampling, YPD medium was supplemented with Penicillin-Streptomycin 100X (BioWest).

For the drop tests experiments, the dilutions were performed on YPD agar plates or in agar plates containing benomyl diluted in DMSO (10 and 25 µg/mL) as well as on control YPD agar plates containing the same amount of DMSO without the drug.

For G1 synchronization experiments, exponentially growing cells were arrested in α-factor (5 µg/mL) at 30 °C. After 1 h and 30 min, α-factor was re-added at the concentration of 2.5 µg/mL and cells were shifted to the restrictive temperature of 37 °C. After 45 min, cells were released in fresh medium at 37 °C and samples at the indicated timepoint were taken for subsequent imaging. For the experiment in Figure S7E, cells were released at 30 °C and after 1 h α-factor was added at the concentration of 20 µg/mL.

METHOD DETAILS

Evolution experiment

Evolution experiment in Figure 1C:

All the colonies evolved were MATa haploid strains. *TUB2/TUB2::KanMX* and *TUB2/tub2^{T238A}::KanMX* diploids were sporulated on SPO plates for 5 days. Tetrad were then dissected on YPD agar plates and the resulting haploid *TUB2::KanMX* and *tub2^{T238A}::KanMX* colonies were selected after respectively 2 and 3 days for growth on G-418 plates and inoculated in 200µL of YPD in a 96-microtiter plate (NUNC—Lifetechnologies) to start parallel independent populations (5 colonies for *TUB2::KanMX* and 21 colonies for *tub2^{T238A}::KanMX*). The day after, cells were shifted in 800 µl of YPD, in a 96-deepwell plate covered with aeraseals (Sigma-Aldrich) at OD₆₀₀ = 0.05 and OD₆₀₀ = 0.1 for WT and *tub2^{T238A}*, respectively. All the populations were cultured in the same 96-deepwell plate and incubated at 30°C under constant orbital shaking on a 96-deepwell block tilted adaptors. The following days and until the end of the evolution experiment cells were grown until stationary phase and daily diluted to OD₆₀₀ = 0.05. The growth rate of each population was assessed by in liquid growth assay every 2–3 days for the entire length of the experiment, except for the first 2 growth assays that were performed at 24 and 48 h from the inoculum. Starting from the 48 h, samples for FACS analysis and glycerol stock were taken at the same timepoints of the growth assays. For each population, the generations g along the length of the evolution experiment were calculated by adding up the number of generations occurred every 24 h, which was calculated according to the following equation:

$$\frac{\log_{10}(\text{OD}_{t24}/\text{OD}_{t0})}{\log_{10}(2)}$$

Where OD_{t0} is the OD value measured right after the daily dilution of the cells, while OD_{t24} is the OD value measured 24 h later.

Evolution experiment in Figure 7D

Five populations were evolved from clones derived from the *tub2^{T238A}* population S12 at generation 36 (from the evolution experiment in Figure 1C). Clones were streaked out on agar plates at 30 °C and inoculated in liquid after 48 h in 200µL of YPD in a 96-microtiter plate. The day after, cells were shifted in 800 µl of YPD, in a 96-deepwell plate. From that moment, cells were kept in culture and their growth rate analyzed as previously explained. At the indicated generations, clones were derived from the five evolved populations and analyzed by Sanger Sequencing and qPCR.

Liquid growth assay

Cells were diluted at $OD_{600} \sim 0.01$ in $200 \mu L$ YPD in a 96-microtiter plate (NUNC—Lifetechnologies) and cultured at $30^\circ C$ overnight and measured every 10 min in a TECAN 200 M Infinite plate reader. For each timepoint, OD_{600} of each well was acquired. The background OD_{600} of the wells filled with clean medium was subtracted from the raw OD_{600} in order to obtain the net OD_{600} . The growth rate (1/h) corresponded to the maximum slope of the curve obtained by plotting the logarithm of the OD values in time.

Drop test assay

Cells were grown overnight at $30^\circ C$ and diluted at the same starting concentration ($OD \sim 0.1/0.2$); they were then diluted 1/10 six times to obtain the following serial dilutions. Every dilution of cells was then spotted on the agar plates.

Colony size analysis

The haploid colonies obtained after three days from the tetrad dissection of the diploids were imaged with a Chemidoc XRS+System (Bio-Rad Laboratories). Colonies were identified as regions of interest (ROIs) by thresholding the digital images with a custom ImageJ script using a Particles Analyzer. Raw colony size is the area in pixels of each ROI. For each dissection plate, the raw colony size was normalized on the mean size of the WT colonies.

Tubulin immunofluorescence

For tubulin staining,⁹ 1mL of overnight growing cells were fixed with 3.7% formaldehyde in KPi buffer (0.1 M Kphos pH6.4 0.5 mM MgCl₂), incubated overnight at $4^\circ C$ and then washed three times with KPi buffer and once with Sorbitol solution (1.2 M Sorbitol, 0.1 M KPi pH 7.4, 0.5 mM MgCl₂). Cell wall was digested at $37^\circ C$ with 200 μL of Sorbitol solution supplemented with 5 μL of zymolyase 10 mg/mL and 0.4 μL of 2- mercaptoethanol for 15/20 min and washed again with Sorbitol solution. 5 μL of spheroplasts were then loaded to glass slides (Thermo Scientific) coated with polylysine (Sigma-Aldrich). After 15/20 min, slides were absorbed in cold MeOH ($-20^\circ C$) for 3 min and subsequently in cold acetone ($-20^\circ C$) for 10 s. Samples were incubated with anti-Tub1 primary antibody (YOL1/34 Bio-Rad) for 2 h at room temperature and washed three times with 1% BSA-PBS. Samples were then incubated with secondary antibody (FITC-conjugated anti-rat antibody from Jackson ImmunoResearch Laboratories, pre-absorbed) for 1 h at room temperature in the dark and washed four times with 1% BSA-PBS. DAPI/antifade (*p*-phenylenediamine 1 mg/ml in PBS adjusted to pH 8.0 and DAPI 0.05 $\mu g/mL$) was added and slides were closed. Images were acquired using DeltaVision Elite imaging system (Applied Precision) based on an inverted microscope (IX71; Olympus) with a camera (CoolSNAP HQ2; Photo-metrics) and an UPlanFL N100x oil immersion objective lens (NA 1.4, Olympus). Using Fiji the sum projection of tubulin fluorescence of 20 Z stacks of 0.2 μm images was performed; a line was drawn along the spindle of each budded cell and the length as well as the mean intensity were measured. The mean intensity of the background was subtracted from the mean intensity of the tubulin signal.

Pairwise comparisons (Figure S1F), were made as explained in the Statistical Analysis section.

Flow cytometry for apparent ploidy/DNA content

Cells were treated according to.⁵² Exponentially growing cells were fixed for 1 h in EtOH 70%, followed by incubation in RNase A solution (0.05 M NaCitrate, 0.25 mg/mL RNase A) for 3 h at $37^\circ C$ and subsequently in proteinase K solution (0.05 M Tris-HCl pH8, 0.01 M CaCl₂, 0.25 mg/mL Proteinase K) overnight at $55^\circ C$. The day after cells were resuspended in Na Citrate solution (0.5M NaCitrate) and sonicated. After staining for 20 min in Sytox Green Solution (1 μM Sytox Green, 0.05 M NaCitrate), samples were acquired using attune cytofluorimeter (Thermo Scientific). Sytox fluorescence was acquired using BL1 laser with a flow rate of 1,000 events/s. The resulting fcs files were analyzed using a customized R script.

Singlets were gated using physical parameters (FSC and SSC). DNA content was computed using the G1 mode of the binned Sytox signal⁵³ with bins whose width is $\sim 1/1,000$ of the instrument range. The median values obtained for the 5 *TUB2* as well as the 21 *tub2*^{T238A} evolving populations were plotted throughout the evolution experiment. At the first timepoint, the median value of the *TUB2* population was used as normalizer.

For Figure S7E, cells were fixed in EtOH 70%, then washed with 50mM TRIS pH7.6 and incubated overnight in 1 mg/mL of RNase A dissolved in 50mM TRIS pH7.6. Samples were then washed in PBS, stained with Propidium Iodide 50 $\mu g/mL$ and acquired using an attune NxT cytofluorimeter (Thermo Scientific).

Flow cytometry for cell size

Cells were treated as for apparent ploidy/DNA content. Beads of 2,4,6 and 10 μm were analyzed by the cytofluorimeter to infer the linear fit between FSC-A values and the bead size. The size of the cells was obtained by plotting the FSC-A values versus the linear fit. The median values of the 5 *TUB2* as well as the 21 *tub2*^{T238A} evolving populations were plotted throughout the evolution experiment.

Sanger sequencing of selected genes

The indicated evolved populations were streaked out on agar plates and grown overnight for 3 days at $30^\circ C$, until visible colonies arose for both *WT* and *tub2*^{T238A}. The colonies were picked and the cells were boiled in 20mM NaOH for 10 min. Colony PCR was done to amplify the gene of interest and the amplification product was analyzed by Sanger Sequencing.

Evaluation of mis-segregation

For the analysis of mis-segregation events,⁹ cells were grown overnight at 30 °C, synchronized in G1 and released at 37 °C. At 90 min from the release, cells were fixed in cold pure EtOH. 100 µL of cells were then dissolved in 900 µL of 50 mM Tris, pH 7.6, sonicated and pelleted; the supernatant was discarded and the pellet resuspended in the small amount of the remaining liquid. 5 µl of cells were loaded on a slide coated with a 2% agar layer. Samples were imaged for ChrV-GFP with DeltaVision Elite imaging system (Applied Precision) based on an inverted microscope (IX71; Olympus), a UPlanFL N 60× (1.25 NA) or 40x (1.30 NA) oil immersion objective lens (Olympus), and a camera (Scientific CMOS Camera). GFP was acquired using single bandpass filters (EX475/28 EM523/36) with 25 z stack (0.2 µm), exposure time 0.5 s, and power lamp 100%. After acquisition, images were deconvolved using SoftWorx. Misseggregation events were scored based on the distribution and number of GFP dots marking chromosome V in the different cell cycle phases⁹ as follows: morphologies of cells defined as missegregated were (i) single cells with more than 1 dot (ii) budded cells with more than 2 dots (iii) re-budded cells with a GFP signal different from 1 dot in the mother and 1 dot in the daughter cell.

DNA extraction

Cells were grown overnight at 30 °C. Then, 1 mL of stationary phase cells were digested at 37 °C with 50 µl of SCE solution (1M Sorbitol, 0.1M NaCitrate, 0.06M EDTA, pH 7.0) supplemented with 2 mg/mL of zymolyase and 8 µl/mL of 2-mercaptoethanol for 30–60 min. Spheroplasts were lysed with 50 µl of SDS solution (SDS 2%, 0.1M Tris-HCl pH 9.0, 0.05M EDTA) for 5 min at 65 °C. DNA was purified with NH₄OAc/isopropanol precipitation, resuspended in 50 µl of H₂O supplemented with 0.25 µl of RNase 10 mg/mL and incubated overnight at 37 °C. DNA was purified again in NH₄OAc/isopropanol, washed in cold EtOH 70% and resuspended in water.

Genomic qPCR on chrXII and chrXVI

Cells were grown overnight on agar plates at 30 °C. Then, a few amounts of cells were picked and boiled in 20 µl of 20mM NaOH for 10 min. As for the qPCR protocol,⁵² forward and reverse primers annealing on the chromosome XII (right arm) or XVI (left arm) were added at a concentration of 5 µM, and LightCycler 480 SYBR Green I Master 2X was finally added to the mix. qPCR was performed with a LightCycler 96 (Roche). The Ct value of the chromosome of interest was normalized on the the Ct value of chromosome 7 (left arm) obtaining a Δ Ct. The raw Δ Ct was normalized on the WT Δ Ct, resulting in the ΔΔ Ct. The 2^{−ΔΔCt} was plotted for each genotype.

For the *tub2*^{T238A} clones from population S12, the error bars are obtained from a t-distribution as explained in⁵⁴

Pairwise comparisons (Figures 6B and 6F), were made as explained in the Statistical Analysis section.

Genomic qPCR on selected genes

Cells were treated as for the genomic qPCR on chrXII and chrXVI. The Ct value of the gene of interest was normalized on the the Ct value of the housekeeping gene RIM1 resulting in the raw Δ Ct. This value was further normalized on the mean *tub2*^{T238A} Δ Ct, resulting in the ΔΔ Ct. The 2^{−ΔΔCt} was plotted for each genotype.

Pairwise comparisons (Figures S5A and S6A), were made as explained in the Statistical Analysis section.

Sequencing and bam files creation

NGS was performed at the Cogentech Unit, using the Illumina flowcell NextSeq 500/550 Mid Output Kit v2.5 (300 Cycles).

Bam files were created according to.⁹ Briefly, FASTA files were trimmed using trimmomatic v0.36⁵⁵ subsequently aligned to reference sequence (sacCer3) using Burrows-Wheeler Aligner (BWA) v0.7.17.⁵⁶ Duplicates were removed using samblaster v0.1.24⁵⁷ and sorted using samtools v1.9.⁵⁸ Finally, bam files were realigned around indels using Picard v2.19.0 (<http://broadinstitute.github.io/picard/>) and GATK v3.8-1⁵⁹ Final bam files have an average depth of coverage of ~50 reads for the NGS at time points T1/Tf of the evolution experiment and of ~10 reads for the NGS of the *tub2*^{T238A} samples involving the varying location of IPL1.

Ancestors populations were clonal.

Analysis of aneuploidy

Depth of coverage was extracted from bam files using a custom script written in python that makes use of the “depth” function contained in the samtools package. Chromosomes were partitioned into bins of 10,000 bp, and the bin-wise median was used for further analysis. We noticed a pronounced bias of depth of coverage apparently related to chromosome length. To detrend the data, we divide the average depth per chromosome in the mutants by the corresponding values in WT.

For the samples of the evolution experiment involving the varying location of IPL1 (Figure S6C), this normalization strategy did not work due to the overall lower coverage. In this case we resorted to an internal control for each sample, as described previously⁹: Plotting chromosome median depth of coverage against chromosome length suggests that this relation can be approximated by an exponential of the form.

$$y = a * \exp(-b * x + c)$$

We fit each sample individually and divided the median depth for each bin by the value corresponding to the respective chromosome resulting from the fit in order to detrend the data. We used robust regression in order to avoid an influence on detrending due to the actual biological signal. Thus, clear aneuploidies are treated as outliers that do not distort the fit. The median of the corrected depth of coverage signal was used as a proxy for chromosomal copy number.

Cumulative ploidy

To plot the cumulative ploidy, we computed the excess of ploidy of the most recurrent chromosomes (IV, XII, XVI). We subtracted 1 from the normalized coverage and set 0 as minimum. In this way, euploid chromosomes would be ~0 and diploid chromosomes higher than 0, depending on the frequency of that particular aneuploidy in the population. We then summed the values obtained for the three chromosomes for each sample.

Identification of single-nucleotide variants and short indels

In order to identify single-nucleotide changes and short indels (less than ~50 bp) by avoiding the variations due to noisy genomic regions or specific to our W303 genetic background, we used the tool IsoMut⁶⁰ as described in.⁹ This tool compares a set of isogenic samples and calls a variant when this is unique for one of the sequences analyzed. We then fed IsoMut with a set of eleven sequences: the target sample sequence, plus 10 technical replicates of wild type yAC4179, in order to remove W303 specific variations or noisy regions. The remaining variations are then joined in a unique database. Using a custom written R script based on VariantAnnotation v1.28.11⁶⁰ the variations were mapped to genomic regions. Following the methods used in,³⁷ we excluded regions annotated in the SGD database as centromeric regions, simple repeats, telomeric regions and LTRs (SGD project; http://downloads.yeastgenome.org/curation/chromosomal_feature/SGD_features.tab, downloaded July 26, 2019). To identify mutations with good signal, we removed those identified by < 5 reads, regardless of their allelic frequency, those with IsoMut cleanliness parameter <0.90, those with IsoMut score <0.21. The mutations found in the mitochondrial DNA were also discarded.

The mutations resulting from this filtering were further screened in order to define candidate mutations.

Identification of candidate mutations and recurrently mutated genes

A *de novo* mutation was identified if it (i) was not present in the ancestor diploids; (ii) was uniquely found in one population; (iii) had a frequency higher than 0.1. We discarded intergenic and synonymous mutations. For both WT and *tub2*^{T238A} strains, genes found mutated by such mutations in at least 2 independent populations, and with a frequency higher than 40% in at least one of these populations, were defined as recurrently mutated genes. For the *tub2*^{T238A}, a further filtering was done by removing from the list of recurrently mutated genes those also found mutated in the WT. Once a gene was recognized as recurrent, every mutation in that gene with a frequency higher than 10% was included in the analysis. even if it was not uniquely found in one population.

QUANTIFICATION AND STATISTICAL ANALYSIS

Statistical analyses were performed using R. Pairwise comparisons (Figures 3B, 3C, 4B, 6A, B, 6D, 6E, 6F, S1F, S3C, S5A, S6A, S6B–S6D, and S6E) were made using a linear model (function `lm`), adjusting for batch effects for experiments performed on different days. Symbols refer to the *p*-values of the coefficient that accounts for the strain effect (ns $p > 0.05$, * $p < 10^{-1}$, ** $p < 10^{-2}$, *** $p < 10^{-3}$, **** $p < 10^{-4}$). The boxplots span the interquartile range (IQR, from the 25th to the 75th percentiles), and the central band represents the median. The lower and upper whisker extends from the box to, respectively, the smallest and largest value no further than 1.5*IQR from the box. Individual measures are plotted as dots.

ADDITIONAL RESOURCES

Estimation of the expected number of mutations in tubulin

Here, we employed standard population genetics tools to address two questions. First we asked whether compensatory mutations in tubulin arising after ~65 generations (Figure 2B) may be compatible with populations size (~10⁷ cells), the total mutation rate $\mu^{tot} = \mu * T_s$ (where $\mu = 1.7 * 10^{-10} gen^{-1}$ the yeast mutation rate (per individual, per nucleotide)³⁷), and T_s , the total number of observed compensatory mutations (31 in total, Figure 2B). Second, we show that the fact that cells likely carry only one tubulin mutation can be explained with diminishing return epistasis.

To address the first point, we evaluated the selection coefficient of the first compensatory mutations, observed in the experiment after about 65 generations (Figure 7C). More in details, we employed the Kimura Fixation probability, $\Pi(s, N) = (1 - e^{-2s}) / (1 - e^{-2Ns})$ ⁶¹, which provides the probability for a mutation with a selection coefficient s to reach fixation in a population of N individuals. The fixation rate (Λ) is then determined by multiplying this probability by the total mutation rate $\Lambda(s, N, \mu^{tot}) = \mu^{tot} * N * \Pi(s, N)$. Using this rate, we calculated the probability of observing at least one mutation after approximately 65 generations. Since all populations show a similar tempo for the increase of growth rate, we assume all 21 lineages exhibit at least one mutation after about 65 generations, similarly to what observed for population 12. Assuming the same selection coefficient for all 31 mutations, we find that an average selection coefficient greater than 0.5 is consistent such experimental observation. These results agree with the observed increase in the growth rate (Figure 1C), which rises from 0.3 h⁻¹ to 0.5 h⁻¹, corresponding to an effective selection coefficient of 0.66. We conclude that our observations align with standard population genetics predictions.

Further, we extended this analysis to investigate the probability of observing a second compensatory mutation, following the fixation of the first one, in the remaining 125 generations until the experiment's conclusion. Since the total frequency of tubulin mutations reaches 100% and does not exceed this value (Figure 2B), our data suggest that each cell carries only one compensatory

mutation in tubulin. This observation implies a significantly lower average selection coefficient compared to the fitness increase caused by the first mutation ($s \leq 0.004$), hence supporting the presence of diminishing returns epistasis.

Mathematical modeling of the euploid scenario

We initially investigated whether the observed replacement dynamics of a disomic population (D) by a euploid population with a compensatory mutation (EM) could be explained simply by competition given the different growth rates of the two strains.

Specifically, let x represent the intra-population frequency of the euploid mutant. We applied a standard mathematical model of population growth with an explicit analytic solution.⁶² In this model, competition between the strains, driven by their different growth rates, is characterized by the selection coefficient $s = \frac{\lambda_{EM}}{\lambda_D} - 1$ where $\lambda_{EM} \approx 0.55 h^{-1}$ and $\lambda_D \approx 0.28 h^{-1}$ (see Figure S7D). The growth dynamics of x are governed by the differential equation:

$$\frac{d}{dt}x(t) = sx(t)(1 - x(t)).$$

We solved this equation by (i) fitting it to observed data points (EM frequency at points 3E, 4E and 5E in Figure 7C) and (ii) imposing as the initial condition for the mutant that at the emergence time $t_{\text{emergence}}$ its intra-population frequency was $x(t_{\text{emergence}}) = 1/N$, with $N = 10^7$ (corresponding to an $OD \approx 1$). Hence, in this model $t_{\text{emergence}}$ was the only free parameter, and we found consistency with experimental data for $t_{\text{emergence}} \approx 30$ gens (Figure 7E).

Next, we considered whether the presence of a single EM cell at 30 gens would be consistent with a scenario where a small number of euploid cells present at the beginning of the experiment could generate a mutant euploid strain within approximately 30 generations. To address this, we used a model describing the probability of emergence of a mutant within a population of exponentially growing cells. For euploid cells, the population growth follows $N_E(t) = N_E(0)\text{Exp}[\lambda_E t]$ where λ_E is the growth rate of euploid cells, and $N_E(0)$ is the number of euploid cells present at $t = 0$ (i.e., at the beginning of the experiment). Euploid cells can generate mutant cells at a mutation rate per division $\mu = \mu_0 * T_s$ where $\mu = 1.7 * 10^{-10} \text{ gen}^{-1}$ is the yeast mutation rate (per individual, per nucleotide)³⁷, and $T_s = 31$, is the total number of observed compensatory mutations observed in *TUB1* and *TUB2* (Table S1).

Following the derivation originally proposed in,⁶³ we model the expected number of established mutants $M(t)$ as:

$$\frac{d}{dt}M(t) = \mu\lambda_E N_E(t).$$

The solution to this equation is:

$$M(t) = \mu N_E(0)(\text{Exp}[\lambda_E t] - 1)$$

This expression provides the expected number of mutants established in an exponentially growing population up to time t . By imposing that at $t_{\text{emergence}} = \frac{30}{\lambda_D} h^{-1}$ (assuming generations are defined as the inverse of the growth rate of disomic strains, which are predominant in the population), the expected number $M(t_{\text{emergence}}) = 1$ gives a condition on the initial number of euploid cells:

$$N_E(0) = \frac{1}{\mu \left(\text{Exp} \left[\frac{30 \lambda_E}{\lambda_D} \right] - 1 \right)}.$$

To compute the initial euploid cell number, we used $\lambda_D \approx 0.28 h^{-1}$ (Figure S7E) and calculated λ_E as follows: (i) the average growth rate at the start of the experiment was observed to $\lambda_{\text{ave}} \approx 0.25 h^{-1}$ (Figure 1C), and (ii) the population at that time consisted of approximately 80% disomic strains (with a growth rate $\lambda_D \approx 0.28 h^{-1}$) and 20% euploid strains (with a growth rate λ_E) (Figure S7A). We find that the numerical value, $\lambda_E \approx 0.16 h^{-1}$ is the solution to the equation $0.2 \lambda_E + 0.8 \lambda_D = \lambda_{\text{ave}}$. With these values, we find $N_E(0) \approx 5$.

Overlapping between compensatory mutations and those detected in patients

We wanted to test whether the tubulin mutations discovered in the evolution experiment show a statistically significant overlap with the tubulin mutations observed in cancer patients. In particular, we focused on β -tubulin (*TUB2*), the most frequently mutated gene in our experiment. To this end, we performed a hypergeometric test in which we gave as input: (i) an upper limit for tubulin mutations detected in yeast and in humans (289, derived from the “Tubulin Mutation Database” [<https://tubulinmutations.bio.uci.edu/>]); (ii) the number of β -tubulin mutations detected in our experiment (21); (iii) the reported mutations detected in cancer patients (same database, 37); the number of mutations that occur both in the evolution experiment and in cancer patients (8). This overlap is statistically significant with a p -value of $p = 0.002$.